On the Factors Controlling the Development of Shallow Convection in Eddy-Diffusivity/Mass-Flux Models

KAY SUSELJ, MARCIN J. KUROWSKI, AND JOÃO TEIXEIRA

Jet Propulsion Laboratory, California Institute of Technology, Pasadena, California

(Manuscript received 23 April 2018, in final form 27 September 2018)

ABSTRACT

This study addresses key aspects of shallow moist convection, as simulated by a multiplume eddy-diffusivity/mass-flux (EDMF) model. Two factors suggested in the literature to be essential for the development of convective plumes are investigated: surface conditions and lateral entrainment. The model consistently decomposes the subgrid vertical mixing into convective plumes and the nonconvective environment. The modeled convection shows low sensitivity to the surface plume area. The results indicate that plume development in the subcloud layer is controlled by both surface conditions and lateral entrainment. Their impact significantly changes in the cloud layer where the surface conditions are no longer important. The development of shallow convection is dominated by the interactions between the plumes and the large-scale field and is sensitive to the representation of the variability of thermodynamic properties between the plumes. A simple two-layer model of steady-state convection is proposed to help understand the role of these processes in shaping the properties of moist convection.

1. Introduction

In state-of-the-art weather and climate models, neither boundary layer turbulence nor moist shallow convection can be explicitly resolved and thus have to be parameterized. One commonly used family of parameterizations that unifies these two regimes is based on the eddy-diffusivity/mass-flux (EDMF) approach, which was initially proposed to represent dry convective boundary layers (Siebesma and Teixeira 2000; Teixeira and Siebesma 2000; Siebesma et al. 2007; Witek et al. 2011a). Note that models by Chatfield and Brost (1987) and Hourdin et al. (2002) represent dry convective boundary layers with some combination of eddy-diffusivity and mass-flux concepts. Over the past few years, several EDMF versions for moist shallow convection have been developed (Soares et al. 2004; Angevine 2005; Rio and Hourdin 2008; Neggers et al. 2009; Neggers 2009; Pergaud et al. 2009; Rio et al. 2010; Sušelj et al. 2012, 2013, 2014). The key concept behind this approach is a formal distinction between strong convective plumes/updrafts, which are responsible for nonlocal mass-flux transport, and the remaining nonconvective environment characterized by local turbulent mixing and parameterized by the eddy-diffusivity model. Although the EDMF approach is relatively new, both the eddy-diffusivity and mass-flux models have been under development for many decades as they are traditionally used to represent vertical mixing in the atmospheric boundary layer and in the moist convective layer in weather and climate models.

The goal of this study is to improve our understanding of the physical mechanisms controlling the development of shallow convection as represented by EDMF parameterizations. To achieve this, we investigate the effects of different EDMF model components and approximations on the accuracy of simulated convection for the well-known Barbados Oceanographic and Meteorological Experiment (BOMEX) case (Siebesma et al. 2003). The EDMF model employed in this study is an improved version of the model documented in Sušelj et al. (2013), with two major modifications.

First, we drop the assumption that the grid-mean thermodynamic variables are equal to their environmental values. This assumption is often used to simplify the formulation of the subgrid fluxes, which are then expressed as a sum of two terms representing the fluxes due to convective plumes and the nonconvective environment (e.g., Siebesma et al. 2007). In a more general formulation of our new model, a third term representing

Corresponding author: Kay Suselj, kay.suselj@jpl.nasa.gov

DOI: 10.1175/JAS-D-18-0121.1

© 2019 American Meteorological Society. For information regarding reuse of this content and general copyright information, consult the AMS Copyright Policy (www.ametsoc.org/PUBSReuseLicenses).

Brought to you by NOAA Central Library | Unauthenticated | Downloaded 03/07/22 07:40 PM UTC

the effects of environmental subsidence (which is typically neglected) is retained in the parameterization of the subgrid fluxes. Furthermore, the eddy-diffusivity component of the subgrid flux is modeled as a function of environmental rather than grid-mean properties.

Second, we design a multiplume mass-flux model with all plumes initialized at the surface. It replaces an older version of the scheme (Sušelj et al. 2013), in which a single bulk plume rooted at the surface was split into multiple plumes at the cloud base. In the early EDMF models, the spectrum of convective plumes has been represented with a single horizontally homogeneous bulk plume (e.g., Angevine 2005; Siebesma et al. 2007; Pergaud et al. 2009; Rio et al. 2010; Witek et al. 2011a). To improve on this approach, recent studies proposed either to account for an internal heterogeneity of the bulk plume (e.g., Jam et al. 2013), to explicitly represent convective updrafts with a multiplume model (e.g., Cheinet 2003, 2004; Sušelj et al. 2013, 2014; Neggers 2015; Sakradzija et al. 2015, 2016) or to merge the two approaches (Sušelj et al. 2012). The key advantage of the multiplume approach is the ability to explicitly account for the nonlinear interactions between the plumes and the environment in a way that a bulk model cannot do.

In multiplume models, each plume is an attempt at representing a collection of similar updraft properties. However, a direct mapping from complex three-dimensional updrafts (like the ones that can be diagnosed from LES) to parameterized plumes is far from straightforward. The behavior of the parameterized plumes depends on a variety of assumptions, in particular, regarding what determines the variability among plumes. Based on these assumptions, multiplume models can be loosely categorized into the following three groups:

1) The variability among plumes is determined at the initialization level. The controlling factors are either the thermodynamic and kinematic plume properties (e.g., Cheinet 2003, 2004; Neggers et al. 2009; Sušelj et al. 2012) or the horizontal sizes of the plumes (e.g., Sakradzija et al. 2015, 2016).
2) The variability among plumes is controlled by processes above the initialization level and can be due to differences in the local environment in which they grow (Brast et al. 2016) or due to stochastic interactions with the environment, which can be represented by stochastic lateral entrainment (Romps and Kuang 2010; Romps 2010; Dawe and Austin 2012; Sušelj et al. 2013, 2014).
3) The variability among plumes is a result of differences in their conditions at the initialization level and of processes above it. Examples include the model presented here and the basic model formulation of Neggers (2015).

Note that in the models from the first group, the differences among the plumes can amplify above the initialization level. This is because the entrainment rate can be a function of a plume's vertical velocity or its horizontal size. Nevertheless, the development and fate of a particular plume is determined at the initialization height, which is not the case for the models from the second and the third groups, for example, because of stochastic processes.

The current model belongs in the third group as the plume properties are designed to depend on both the different surface thermodynamic and kinematic properties and stochastic entrainment. The surface properties are formulated as in Cheinet (2003). The stochastic entrainment parameterization is qualitatively consistent with the ideas proposed by Krueger et al. (1997) and Romps and Kuang (2010).

We here examine which of the two processes is more important for the vertical development of the plumes. We also design an experiment in which the parameterization of the two processes is gradually simplified to find the key physical components of the scheme that allows realistic representation of shallow convection. Finally, to understand the results of these simulations, we formulate a simple two-layer model for steady-state convection to explain how interactions between the plumes and the environment affect the properties of convection.

The paper is organized as follows. Section 2 (and appendix A) describes the new EDMF model, with a special emphasis on the introduced modifications with respect to our earlier model (Sušelj et al. 2013). In section 3, we examine the sensitivity of the model to surface updraft area (UA), investigate the impact of different components on the representation of convection, and formulate a two-layer steady-state model to explain the simulated variability. A summary and conclusions are given in section 4.

2. Model overview

Our framework is a stochastic multiplume EDMF model that derives from Sušelj et al. (2013), with some crucial modifications described below. Appendix A provides further details.

The EDMF model is implemented into a single-column model (SCM) that serves as a test bed. The SCM solves equations for the mean moist conserved variables (liquid water potential temperature $\theta_l \equiv \theta - L_v c_p^{-1} q_l$ and total water $q_t \equiv q_v + q_l$), the two components of horizontal momentum (u and v), and turbulent

Brought to you by NOAA Central Library | Unauthenticated | Downloaded 03/07/22 07:40 PM UTC

kinetic energy (TKE; e).[1] A generic Reynolds-averaged conservation equation for a prognostic variable $\overline{\varphi}$ can be written as

$$\frac{\partial \overline{\varphi}}{\partial t} = -\frac{1}{\rho}\frac{\partial}{\partial z}(\rho \overline{w'\varphi'}) - \sum_{k=1}^{3} \overline{u}^k \frac{\partial \overline{\varphi}}{\partial x^k} + \overline{S}_\varphi, \tag{1}$$

where $\varphi = \{\theta_l, q_t, u, v, e\}$ represents any of the five prognostic variables, $x_k = \{x, y, z\}$ the two horizontal and the vertical directions, $u^k = \{u, v, w\}$ the velocities along these directions, and S_φ is a source/sink term. In Eq. (1), horizontal gradients of subgrid fluxes are neglected as is typically done for models with horizontal resolutions of ~1 km or coarser.

In this multiplume EDMF framework, the subgrid domain is divided into $i = 1, \ldots, I$ horizontally homogeneous convective plumes, each with a fixed fractional area (from the surface up to its termination height) and the remaining nonconvective environment.

If a_i and a_e represent horizontal fractional areas of the ith plume and the environment, then the total fractional area of all the components by definition equals unity:

$$\sum_{i=1}^{I} a_i + a_e = 1. \tag{2}$$

The grid-mean value of a prognostic variable $\overline{\varphi}$ is the area-weighted sum of the values for the plumes and environment:

$$\overline{\varphi} = \sum_{i=1}^{I} a_i \varphi_i + a_e \varphi_e, \tag{3}$$

where the subscripts i and e refer to the plumes and the environment, respectively. The subgrid covariance between any two model variables, φ and ψ, can be written as (Wang and Stevens 2000; Chinita et al. 2018)

$$\overline{\varphi'\psi'} = a_e \overline{\varphi'\psi'}\big|_e + a_e(\varphi_e - \overline{\varphi})(\psi_e - \overline{\psi}) + \sum_{i=1}^{I} a_i \overline{\varphi'\psi'}\Big|_i + \sum_{i=1}^{I} a_i(\varphi_i - \overline{\varphi})(\psi_i - \overline{\psi}) \tag{4}$$

where the $\overline{\varphi'\psi'}|_e$ and $\overline{\varphi'\psi'}|_i$ terms represent the covariance of φ and ψ in the environment and in the ith plume, respectively.[2] Because the plumes are assumed to be horizontally homogeneous, the covariance between variables within each individual plume is zero, leading to

$$\overline{w'\varphi'} = a_e \overline{w'\varphi'}\big|_e + a_e(w_e - \overline{w})(\varphi_e - \overline{\varphi}) + \sum_{i=1}^{I} a_i(w_i - \overline{w})(\varphi_i - \overline{\varphi}), \tag{5}$$

where the subgrid vertical flux is a sum of three components that represent, respectively, the small-scale mixing in the environment (usually called eddy diffusivity), the vertical mass flux of the subsiding environment, and the vertical mass flux of convective plumes. The second term is typically neglected in EDMF models, including Sušelj et al. (2013), following the assumption of small plume area, for which the environmental and grid-mean values are equal.

The small-scale mixing in the environment is parameterized with the eddy-diffusivity approach:

$$\overline{w'\varphi'}\big|_e = -K_{m/h,e}\frac{\partial \varphi_e}{\partial z}, \tag{6}$$

where $K_{m/h,e}$ represents the eddy viscosity or diffusivity coefficient for the environment (whose ratio is a function of the Richardson number; see appendix A). The current model does not represent condensation in the nonconvective environment, which for the shallow convection cases considered herein can be neglected.

Using Eqs. (2), (3), (5), and (6), the equation for subgrid fluxes can be written as

$$\overline{w'\varphi'} = -\alpha_\varphi \frac{\partial \overline{\varphi}}{\partial z} - \beta_\varphi \overline{\varphi} + \gamma_\varphi, \tag{7}$$

with

$$\alpha_\varphi = \frac{K_{\varphi,e}}{1 - \sum_{i}^{I} a_i}, \tag{8}$$

$$\beta_\varphi = \frac{\sum_{i=1}^{I} a_i(w_i - \overline{w})}{1 - \sum_{i=1}^{I} a_i} + K_{\varphi,e}\frac{\partial}{\partial z}\left(\frac{\sum_{i=1}^{I} a_i}{1 - \sum_{i=1}^{I} a_i}\right), \tag{9}$$

$$\gamma_\varphi = \sum_{i=1}^{I} a_i w_i \varphi_i + \frac{\left(\sum_{i=1}^{I} a_i \varphi_i\right)\left(\sum_{i=1}^{I} a_i w_i - \overline{w}\right)}{1 - \sum_{i=1}^{I} a_i} + K_{\varphi,e}\frac{\partial}{\partial z}\left(\frac{\sum_{i=1}^{I} a_i \varphi_i}{1 - \sum_{i=1}^{I} a_i}\right), \tag{10}$$

[1] See appendix B for the list of symbols.

[2] For example, $\overline{\varphi'\psi'}|_e \equiv \overline{(\varphi - \overline{\varphi}_e)(\psi - \overline{\psi}_e)}^e$, where the overbar with the subscript e denotes the average over the environment. Similar equation can be written for each of the ith plumes.

Brought to you by NOAA Central Library | Unauthenticated | Downloaded 03/07/22 07:40 PM UTC

where $K_{\varphi,e}$ represents either the eddy diffusivity (for $\varphi = \{\theta_l, q_t\}$) or eddy viscosity (for $\varphi = \{u, v\}$) coefficient. The prognostic equations, using Eqs. (7)–(10), are integrated with a single (i.e., without any time- or process-splitting approximation) forward-in-time semi-implicit numerical solver. In the solver, only the variables α_φ, β_φ, and γ_φ from Eq. (7) are treated explicitly in time.

Other significant differences between this new EDMF version and the one described in Sušelj et al. (2013) are as follows. Instead of splitting a single bulk dry plume into multiple moist plumes at cloud base, the new model initializes all plumes at the surface. Each of them is independently integrated in the vertical as long as its plume velocity remains positive. Condensation within a plume occurs when its total water mixing ratio exceeds the saturated water vapor mixing ratio. The ensemble of subgrid plumes can, therefore, include both dry and partly moist convective plumes, with their individual properties depending on both surface properties and interactions with the environment (i.e., through lateral entrainment).

To specify the surface conditions for the plumes, we first assume that the near-surface variability of the vertical velocity and the thermodynamic fields (i.e., virtual potential temperature and total water mixing ratio) follow a joint-normal probability density function (PDF) and that their higher moments can be represented by the surface-layer scaling laws. The plumes are thought to represent the right tail of this marginal vertical velocity PDF. The near-surface vertical velocity of an individual plume is computed by discretizing the tail of the marginal vertical velocity PDF into I equidistant vertical velocity bins. The near-surface virtual potential temperature and total water mixing ratio are computed as an average value of the corresponding variable over the vertical velocity bin, and the fractional area is an integral of the vertical velocity PDF over the bin size. This parameterization is similar to that from Cheinet (2003), with the details described in appendix A.

The entrainment rate formulation is the same for both dry and moist parts of the plume. The lateral entrainment is a discrete stochastic process, and the entrained air has the grid-mean properties, which assumes some interactions between the plumes (see appendix A for details). When a plume travels a distance dz, the probability of an entrainment event is assumed to be proportional to that distance. Consequently, the number of entrainment events between two vertical model levels follows a Poisson distribution. A fixed amount of environmental air is assumed to be entrained into the plume during each entrainment event. This approach was previously used for the cloud layer (Sušelj et al. 2013) and partly follows the works of Krueger et al. (1997) and Romps and Kuang (2010). Additionally, the entrainment length scale (i.e., the average distance that a plume needs to travel to entrain once) is computed as a function of the surface convective velocity scale instead of the depth of the convective layer.

In the main simulations presented herein, we set $I = 100$. Therefore, an ensemble of convective updrafts is represented by 100 plumes per model time step. Each plume is characterized by its own set of surface conditions and stochastically computed profiles of entrainment rates. Such a Monte Carlo method introduces some statistical noise, which is however reduced in time-averaged results. In section 3a, we investigate the intermittency of convective properties resulting from this statistical noise.

In the SCM model, the large-scale horizontal advection terms, radiative fluxes, surface fluxes, geostrophic wind, and the initial conditions are all prescribed. The model equations are solved on a vertically staggered grid with the mean thermodynamic variables and horizontal wind components defined on midlevels and the TKE and the plume properties defined on full levels. The vertical resolution of the SCM and the time step in all experiments are 20 m and 20 s, respectively.

We investigate the EDMF model behavior for the BOMEX case (Siebesma et al. 2003). The BOMEX case is an example of quasi-steady marine shallow convection with a well-mixed subcloud layer capped by a shallow cumulus layer. The cloud base is located around 500 m, and the cloud layer extends up to nearly 2000 m. The initial conditions, forcing (i.e., surface fluxes, advection of dry air in the subcloud layer, radiative cooling, and the large-scale vertical velocity) and the LES reference results for the comparison are taken from Siebesma et al. (2003).

3. Results

a. *Sensitivity to surface updraft area and number of plumes*

Figure 1 compares grid-mean profiles of thermodynamic moist conserved variables: liquid water potential temperature θ_l and total water mixing ratio q_t, as well as their subgrid vertical fluxes, for eight EDMF simulations characterized by the surface UAs ranging from 1% to 50%, averaged between the second and the third simulation hours. Different surface UAs were obtained by modifying the minimum near-surface vertical velocity represented by the updrafts (i.e., the parameter $w_{\min}$; see appendix A). Since the vertical velocity distribution is assumed to be normal with zero mean, the surface UA cannot exceed 50% as the updrafts are by definition associated with positive vertical motions. The SCM

Brought to you by NOAA Central Library | Unauthenticated | Downloaded 03/07/22 07:40 PM UTC

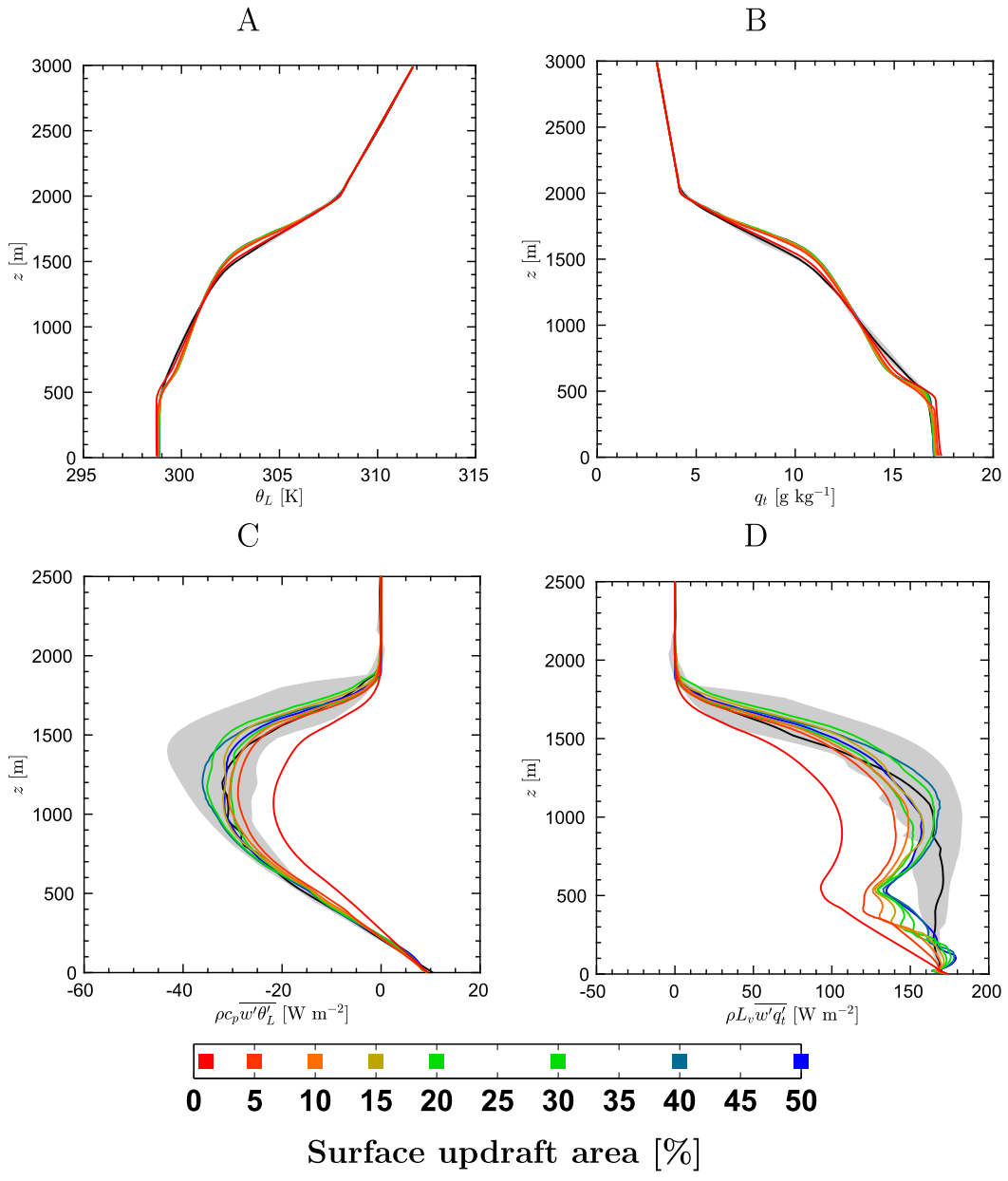

FIG. 1. Profiles of mean moist conserved variables: (a) liquid water potential temperature, (b) total water mixing ratio, and (c),(d) their subgrid vertical fluxes for different surface updraft areas shown in the legend. Black lines represent the LES ensemble-mean results, and the gray areas represent the interquartile range from the LES. All the profiles are averaged across the second and third simulation hours.

results are compared with the LES ensemble data from Siebesma et al. (2003). The key result from Fig. 1 is that almost all EDMF simulations well represent the profiles of thermodynamic variables owing to realistic representations of their subgrid fluxes. Moreover, the profiles of moist conserved variables and their subgrid fluxes show little sensitivity to the large changes in the surface UA. An exception is the simulation with the lowest surface UA (i.e., 1%), which notably underestimates the vertical fluxes in the entire convective layer. While the LES flux of total water mixing ratio is almost constant with height, the EDMF flux tends to reach a local minimum around the cloud base. This feature is also present in some other models (e.g., Cheinet 2004). We performed additional sensitivity experiments (not shown) to conclude that the moisture flux profile can be improved by increasing the updraft velocity [e.g., by modifying the constants a_w and b_w in Eq. (A14)].

Brought to you by NOAA Central Library | Unauthenticated | Downloaded 03/07/22 07:40 PM UTC

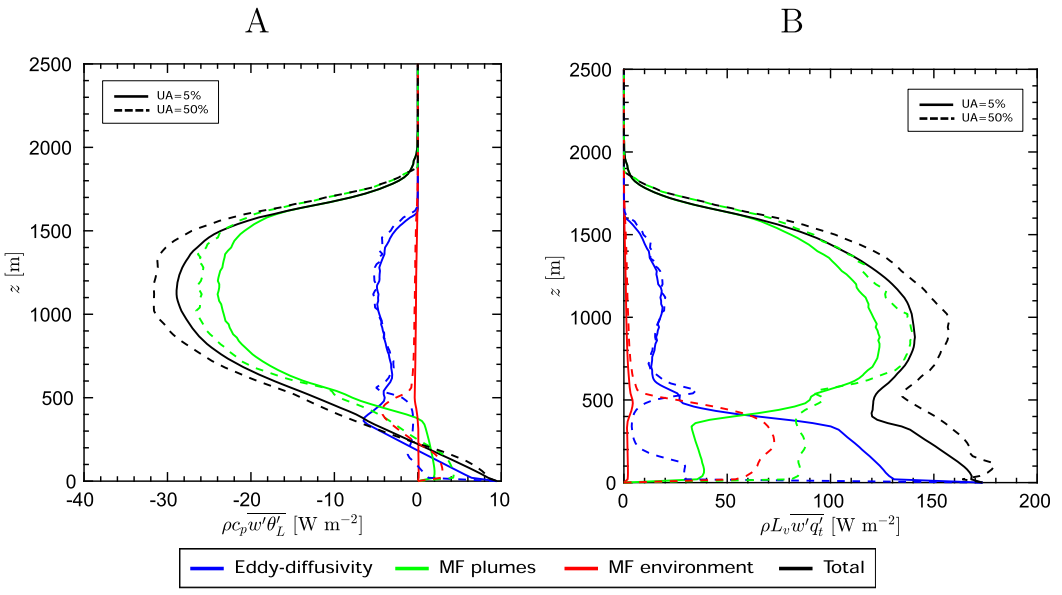

FIG. 2. Profiles of the subgrid vertical flux components: eddy diffusivity (blue), mass flux due to convective plumes (green), mass flux due to a subsiding environment (red), and the sum of the three components (black) (a) for liquid water potential temperature and (b) for total water mixing ratio. Solid and dashed lines denote the results for the surface UA of 5% and 50%, respectively.

However, such modifications deteriorate the representation of moist convection in the cloud layer and are omitted in this study. The profiles of moist conserved variables and turbulent fluxes do not change in any noticeable way in the following four simulation hours, the exception being the results of the experiment with the smallest surface UA. In this case, the subcloud layer and the lower cloud layers become significantly colder and moister and the cloud layer becomes warmer and dryer. This result is consistent with an underestimation of the subgrid fluxes for this experiment.

Figure 2 shows the partitioning of the EDMF subgrid fluxes of moist conserved variables into the three components [i.e., eddy diffusivity, mass flux of convective updrafts, and mass flux of the subsiding environment; see Eq. (5)] for two experiments with very different surface UAs of 5% and 50%. For both experiments, the subgrid fluxes in the cloud layer (between 200 and 500 m above cloud base) are dominated by convective updrafts. On the contrary, the results in the subcloud layer strongly depend on the surface UA. For the surface UA of 5%, the eddy-diffusivity term dominates the subgrid fluxes. For the surface UA of 50%, eddy diffusivity becomes small, and the other two components dominate. While it is evident that convective updrafts represent most of the turbulence in the cloud layer (e.g., Siebesma et al. 2003), it is less clear how the subgrid fluxes should partition in the subcloud layer. For example, Lappen and Randall (2001) suggest that turbulence in the subcloud layer is dominated by nearly symmetric vertical motions seen as a relatively small skewness of vertical velocity. Our EDMF results qualitatively agree with these findings. In the experiments with small surface UAs, the dominant eddy-diffusivity component is assumed to represent isotropic turbulent motions. For large surface UAs, fractional areas and magnitudes of vertical velocity in the updrafts and the environment are similar because most of the updrafts survive to the cloud base (as shown below). Therefore, the updrafts and environment collectively represent quasi-symmetric turbulent motions with each accounting for approximately 50% of the turbulent flux. Accounting for this effect is only possible after including the term representing mass flux of the subsiding environment.

To investigate the reason for the small sensitivity of the convective mass flux to the surface UA, Fig. 3 compares the area-weighted mean properties of moist updrafts from EDMF against the cloud and cloud-core LES ensemble means.[3] The compared properties include the conditionally averaged updraft fractional area, vertical velocity, perturbations of moist conserved thermodynamic variables, cloud water mixing ratio, and

[3] Cloud-averaged LES fields account for all cloudy grid points, while more restrictive cloud-core-averaged fields account for all cloudy grid points with positive buoyancy with respect to the slab mean.

Brought to you by NOAA Central Library | Unauthenticated | Downloaded 03/07/22 07:40 PM UTC

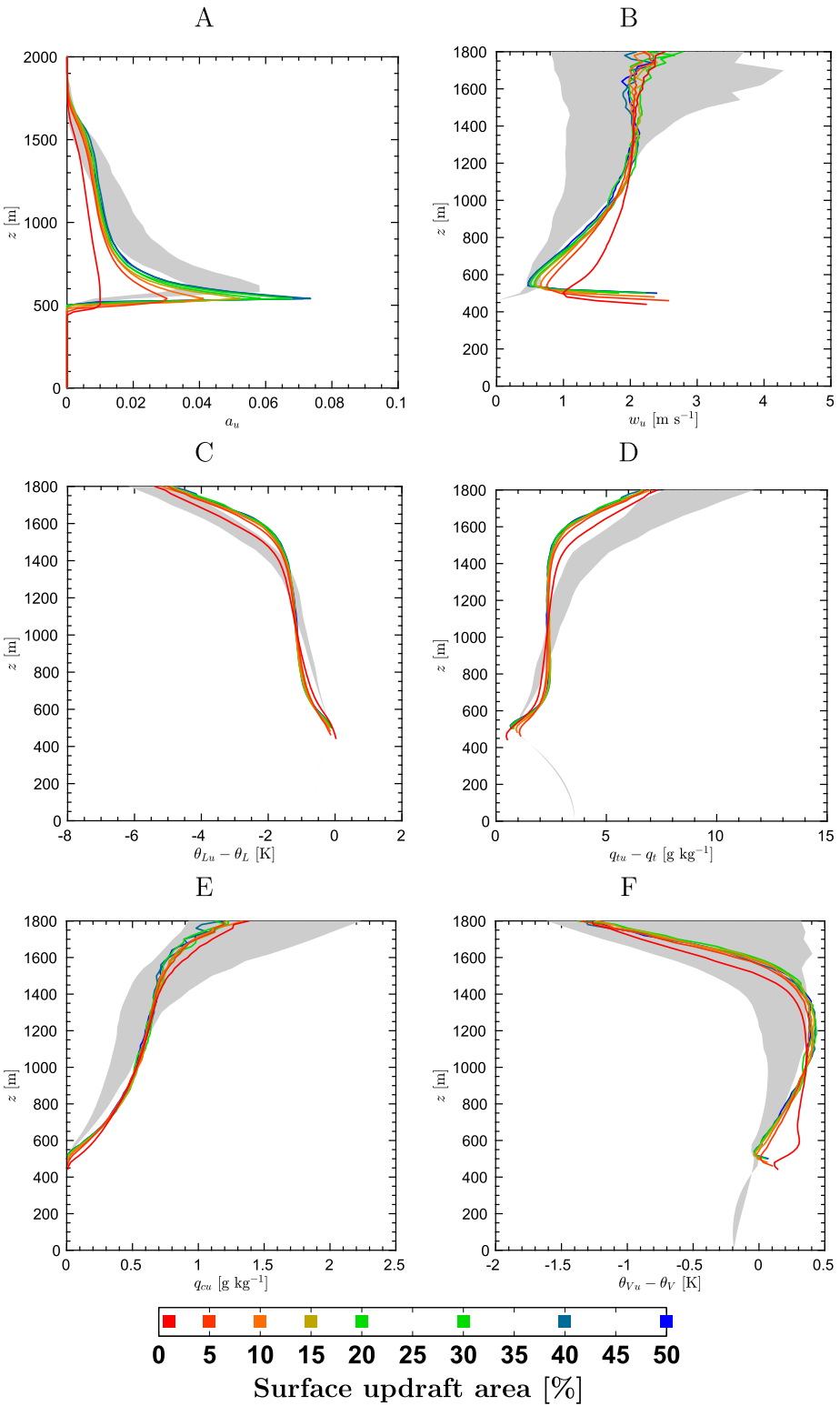

FIG. 3. Mean properties of moist updrafts: (a) fractional area, (b) vertical velocity, (c),(d) excesses of moist conserved variables from their slab means, (e) liquid water mixing ratio, and (f) excess of virtual potential temperature, for different surface updraft areas in the EDMF model, as shown in the legend. Black lines represent the LES ensemble means, and the gray shading shows the interquartile range from the LES results. All the profiles are averaged across the second and the third simulation hours.

Brought to you by NOAA Central Library | Unauthenticated | Downloaded 03/07/22 07:40 PM UTC

virtual potential temperature perturbation. The diagnosed LES updraft areas peak between 4% and 6% at the height of around 600 m, and they gradually decrease toward the cloud top (~2000 m). This decrease results from a gradual termination of the updrafts with height, as the horizontal area of individual updrafts is constant. The corresponding EDMF profiles converge to similar values (except for the simulation with the surface UA of 1%) with the cloud-base peak ranging between 3% and 7%. For all EDMF simulations, dry updrafts do not penetrate into the cloud layer. They either condense and continue to rise as moist updrafts or terminate (not shown). Consequently, mean moist updraft velocity increases with height along with both the amount of cloud condensate and the excess of total moisture (with respect to the grid mean), while the liquid water potential temperature perturbations decrease with height. The profiles of virtual potential temperature perturbation show that the updrafts are on average marginally buoyant from the cloud base to the height of around 1500 m. From above 1500 m up to the cloud top, a significant number of updrafts overshoot their neutral buoyancy, which results in the negative updraft virtual potential temperature perturbation at that height. Again, the profiles from all eight EDMF simulations are almost the same regardless of the large changes in the surface UA. Even using the unrealistically small surface UA of 1% yields reasonable results; however, updraft area is underestimated while vertical velocity and virtual potential temperature perturbations are both overestimated in the lower part of the cloud layer. These results are consistent with the idea that the updrafts represent only the strongest surface plumes, which are associated with the most active convective clouds above the saturation level.

In Figs. 4a and 4b, we show two metrics summarizing the properties of cloud layer: convective cloud cover (CC) and liquid water path (LWP) for the experiments with a different number of surface updrafts. The CC is simply the maximum convective cloudiness over the vertical dimension, which follows from the assumption that convective clouds are maximally overlapped, and LWP is computed from liquid water in convective updrafts. Results are averaged between the second and the sixth simulation hours to reduce temporal variability and because the BOMEX case is in quasi-steady state. In the experiments with the surface UA smaller than around 2%, all updrafts condense, and therefore, CC equals the surface UA. When the surface UA increases above this value, a gradually smaller fraction of the updrafts condenses so that CC slowly increases to approximately 5%. For LWP, its values are somewhat larger than for LES, and they remain relatively independent of the surface UA as long as the latter is higher than around 5%. The time-averaged results from the experiments with a significantly different number of surface updrafts differ only marginally. However, using a smaller number of updrafts generally yields noisier results.

This noise is presumably associated with stochastic entrainment that leads to some intermittency of the modeled convection. Figures 4c and 4d show a measure of this intermittency (i.e., the normalized standard deviations) for the moist updraft area and the subgrid vertical flux of the total water mixing ratio in the upper cloud layer (between 1600 and 1700 m) as a function of the prescribed number of surface updrafts, for two sets of experiments with different values of surface UAs. We show the results for the upper cloud layer as the UA there is small and therefore the intermittency of convective properties is the greatest. The results show that the two standard deviations decrease approximately in a power-law relation to the number of updrafts. The intermittency of the subgrid flux of total water is dominated by the intermittency of the moist updraft area. The normalized standard deviation of the subgrid flux for liquid water potential temperature (not shown) is similar to the one for the total water mixing ratio. The results also suggest that the intermittency increases with the surface UA and that moist convection can be modeled with a small number of updrafts but at the expense of the intermittency of the results.

b. *What controls plume development?*

Arguably, the realistic representation of moist updraft properties by EDMF is due to simulating the realistic spread of the thermodynamic and kinematic variables for the ensemble of updrafts. Two model components can be responsible for this spread: (i) differences in the updraft initial (i.e., surface) conditions and (ii) stochastic entrainment. At first glance, the results shown in section 3a indicate that the parameterization of updraft initial conditions is crucial for this spread, which would agree with some previous studies (e.g., Cheinet 2003; Neggers et al. 2009). According to this hypothesis, only updrafts with the highest surface vertical velocity, buoyancy, and moisture (i.e., those that represent the highest several percent of the near-surface vertical velocity distribution) reach the condensation level. As the updrafts rise farther into the cloud layer, the weaker surface updrafts terminate first, and only the strongest surface updrafts reach the top of that layer. Therefore, with the increase of surface UA, a larger fraction of weaker updrafts from the prescribed surface joint PDF is incorporated into the mass-flux scheme. These weaker updrafts presumably terminate in the subcloud layer and do not reach the condensation level. If this hypothesis were correct, then the role of stochastic entrainment for

Brought to you by NOAA Central Library | Unauthenticated | Downloaded 03/07/22 07:40 PM UTC

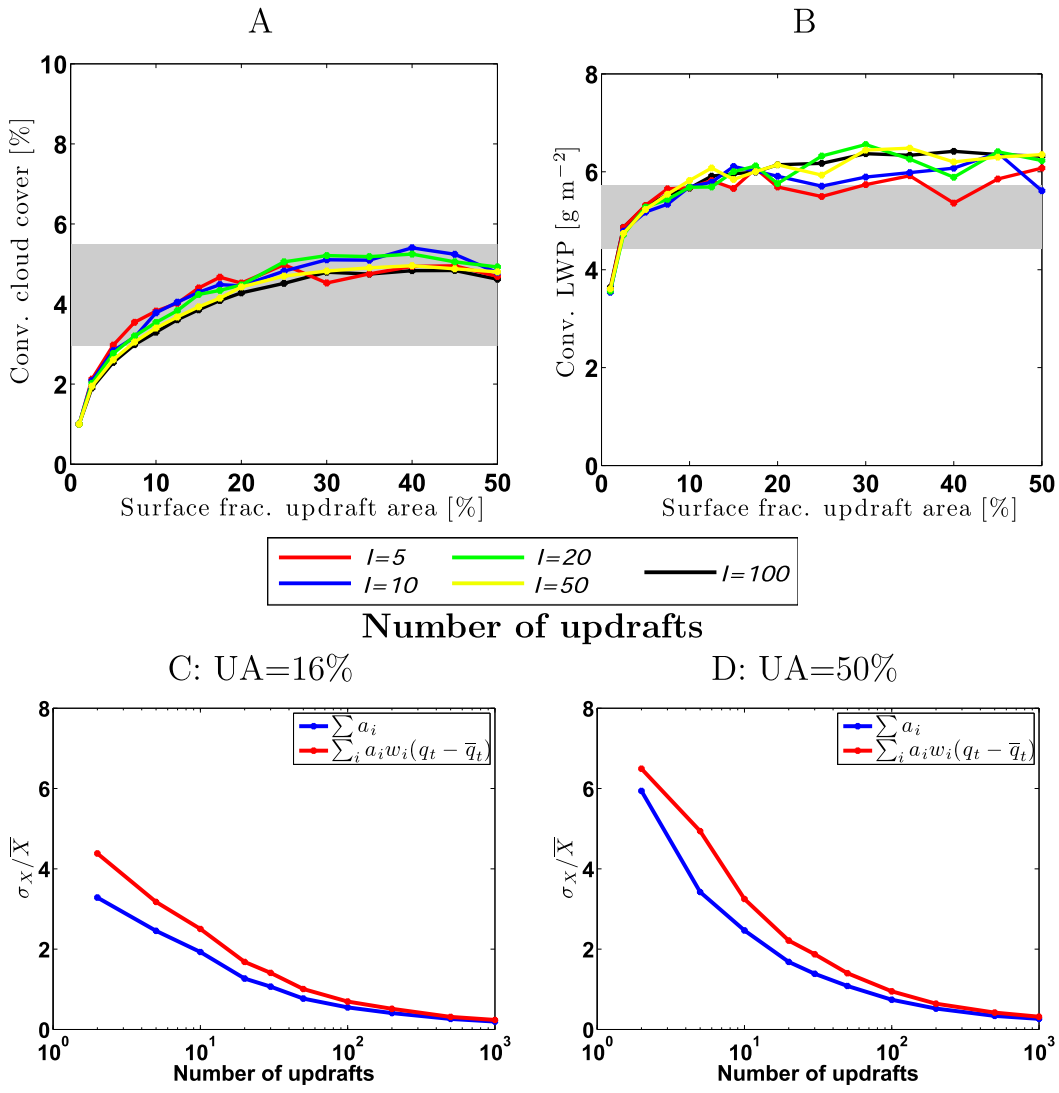

FIG. 4. (a) Updraft cloud cover and (b) LWP as a function of the surface UA and their dependence on the number of surface plumes. Each colored line represents a set of experiments for a fixed number of plumes, as shown in the legend. The gray shading represents the interquartile range from LES. (c),(d) Temporal standard deviation of the moist updraft area and the subgrid vertical flux of total water mixing ratio normalized by their mean and averaged over the upper cloud layer (the heights of 1600 and 1700 m) as a function of the number of surface plumes for experiments with the surface UA of (c) 16% and (d) 50%. All the results are averaged from the second through the sixth simulation hours.

the spread of the updraft properties would be insignificant, and its parameterization could be simplified.

To quantify the role of the two elements (i.e., updraft surface conditions and entrainment rate) on the updraft termination height, we introduce two new metrics: surface updraft index and integrated entrainment rate. The surface updraft index corresponds to the parameter i in Eqs. (A15)–(A18) and numbers the bins of the surface PDFs used to initialize updrafts. Therefore, updrafts with higher surface indices are characterized by higher near-surface vertical velocity, buoyancy, and moisture. The normalized integrated entrainment rate $\tilde{\varepsilon}_i$ for the ith updraft is defined as the difference between the vertically integrated entrainment rate of the ith updraft and that of a hypothetical average updraft, normalized by the square root of variance of the average updraft:

$$\tilde{\varepsilon}_i(z) = \frac{\int_0^z (\varepsilon_i - \langle\varepsilon\rangle)\, dz}{\left[\mathrm{Var}\left(\int_0^z \varepsilon\, dz\right)\right]^{1/2}} = \frac{\int_0^z \varepsilon_i\, dz - \varepsilon_0 z/L_\varepsilon}{\varepsilon_0\sqrt{z/L_\varepsilon}}, \quad (11)$$

Brought to you by NOAA Central Library | Unauthenticated | Downloaded 03/07/22 07:40 PM UTC

where $\langle\varepsilon\rangle$ represents the average of the PDF of entrainment rates and Var denotes the variance. To arrive at the final expression, we consider the entrainment rate following Eq. (A22). The entrainment rate and the variance of the hypothetical average updraft are computed as follows:

$$\int_0^z \langle\varepsilon\rangle\, dz = \lim_{\Delta z\to 0}\sum_{k=1}^{z/\Delta z}\frac{\varepsilon_0}{\Delta z}\langle\mathscr{P}_k(\Delta z/L_\varepsilon)\rangle\Delta z = \varepsilon_0 z/L_\varepsilon, \tag{12}$$

$$\begin{aligned}\mathrm{Var}\left(\int_0^z \varepsilon\, dz\right) &= \mathrm{Var}\left[\lim_{\Delta z\to 0}\sum_{k=1}^{z/\Delta z}\frac{\varepsilon_0}{\Delta z}\mathscr{P}_k(\Delta z/L_\varepsilon)\Delta z\right]\\ &= \lim_{\Delta z\to 0}\sum_{k=1}^{z/\Delta z}\mathrm{Var}\left[\varepsilon_0\mathscr{P}_k(\Delta z/L_\varepsilon)\right]\\ &= \varepsilon_0^2 z/L_\varepsilon\end{aligned} \tag{13}$$

where $\mathscr{P}(\lambda)$ represents a random number from the Poisson distribution described by the λ parameter. Note that both mean and variance of the Poisson distribution are equal to λ. To derive the expression after the second equal sign in Eq. (13), we use the fact that the Poisson distributions at different levels k are independent of each other. In the definition of the normalized entrainment rate, we use the integrated entrainment rate rather than the entrainment rate itself because the updraft properties at a certain model level are more closely related to the vertically integrated entrainment rate (i.e., from the surface up to that level) than to the entrainment rate at that model level.

Figure 5 shows the frequency of occurrence of the updraft surface index and the integrated entrainment rate as the functions of height. To improve their statistical significance, we analyze the updraft properties for 10 model runs. Two sets of plots are shown for the simulations using surface UAs of 16% and 50%. For the value of 16%, the updrafts represent the near-surface vertical velocities exceeding one standard deviation of the assumed PDF.

For the smaller surface UA (Fig. 5a), all the updrafts are equally likely to reach the mean cloud-base height (located at around 500 m, although individual updrafts may condense at slightly different heights) regardless of their surface indices. This can be seen through the uniform frequency distribution ($1/I = 0.01$) for all hundred indices within this layer. A large fraction of these updrafts terminate in the layer between cloud base and the level of maximum cloudiness (~100 m into the cloud layer; not shown) before they condense. Note that above the level of maximum cloudiness, the structure of the PDFs abruptly changes. Frequencies of occurrence of the updrafts with larger surface indices increase at the expense of frequencies of the updrafts with smaller surface indices. In other words, stronger surface updrafts have a higher chance of reaching the level of maximum cloudiness.

Incorporating weaker updrafts into the mass-flux model (i.e., for the 50% surface UA) modifies this picture since the surface updraft index more strongly determines which of the updrafts penetrate into the cloud layer (Fig. 5b). For this simulation, updrafts with lower surface indices start terminating at lower heights compared to the previous simulation, and almost none of the updrafts with index lower than 30 reach the height of maximum cloudiness.

In terms of the normalized entrainment rate (Figs. 5c,d), the subcloud values are significantly larger than their in-cloud counterparts. Also, a notable transition for the entrainment rate from a wide subcloud distribution to a narrow in-cloud distribution occurs near the cloud base. These results indicate that the entrainment rate plays a crucial role in the termination of updrafts. Namely, the entrainment rate is inversely correlated with the termination height. Figures 5c and 5d also show that for both simulations virtually none of the updrafts entraining more than the hypothetical average updraft can survive above the height of 600 m. This can be seen as a near-zero frequency of the positive integrated entrainment rates in this layer. In fact, the mean integrated entrainment rate for the updrafts that survive to the level of 600 m is about one standard deviation smaller than that of the hypothetical average updraft. Although the results for both surface UAs are similar, their mean profiles (Fig. 5e) differ within the cloud layer, with smaller entrainment rates for larger UA. Note that the denominator in Eq. (11) increases with height; therefore, if the integrated entrainment rate is constant at any height or is decreasing with height, only the updrafts that entrain less than the hypothetical average updraft at that height penetrate into the level above.

These results indicate that, in general, lower entrainment rates and larger initial buoyancy (and thus vertical velocity and moisture from the joint PDF) both increase an updraft's chances of reaching higher altitudes. They also indicate that these two factors determine which updrafts are most likely to terminate near the cloud base. However, once the updrafts reach the level of maximum cloudiness, their termination height becomes almost entirely dependent on the entrainment rate. This can be concluded from the fact that the frequency of occurrence for the surface index remains almost constant above 600 m. The above analysis contradicts our working hypothesis, in which only the updrafts with the strongest surface vertical velocity, buoyancy, and moisture condense. The documented behavior of the EDMF

Brought to you by NOAA Central Library | Unauthenticated | Downloaded 03/07/22 07:40 PM UTC

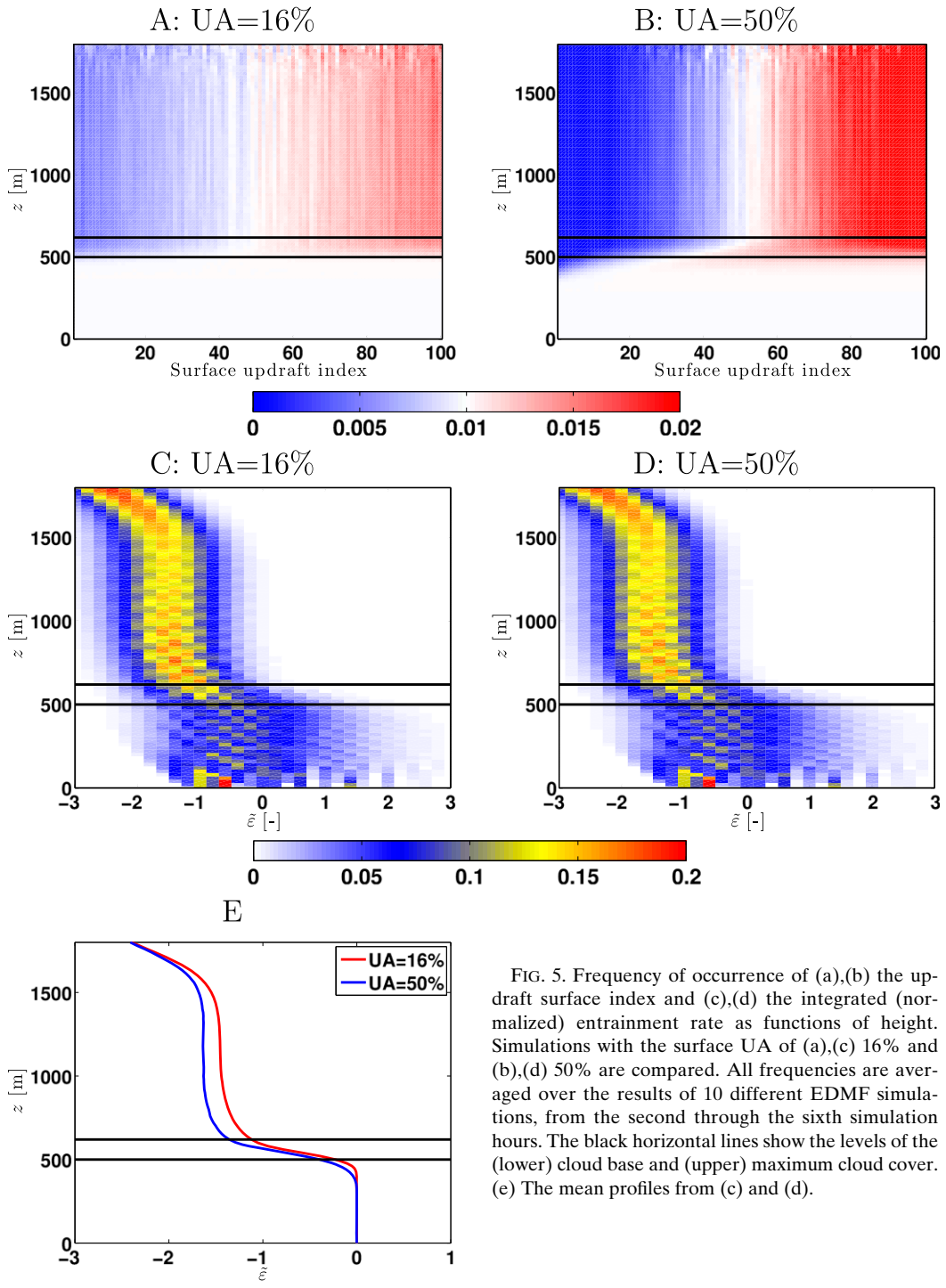

FIG. 5. Frequency of occurrence of (a),(b) the updraft surface index and (c),(d) the integrated (normalized) entrainment rate as functions of height. Simulations with the surface UA of (a),(c) 16% and (b),(d) 50% are compared. All frequencies are averaged over the results of 10 different EDMF simulations, from the second through the sixth simulation hours. The black horizontal lines show the levels of the (lower) cloud base and (upper) maximum cloud cover. (e) The mean profiles from (c) and (d).

model is in a qualitative agreement with the LES results from Romps and Kuang (2010). In particular, they found that thermodynamic properties of moist updrafts depend on their ''nature'' (i.e., surface conditions) only for a few hundred meters above the cloud base, while the ''nurture'' (i.e., lateral entrainment) dominates aloft.

c. *Sensitivity to parameterizations of surface conditions and entrainment*

To determine which elements in the formulation of the surface conditions and the entrainment rate are the most critical for the development of convection, we perform a set of numerical experiments, in which the

Brought to you by NOAA Central Library | Unauthenticated | Downloaded 03/07/22 07:40 PM UTC

TABLE 1. List of EDMF experiments.

Experiment name	Entrainment rate parameterization	Surface updraft conditions
Control	$\varepsilon_i(\Delta z) = \frac{\varepsilon_0}{\Delta z}\mathscr{P}_i\left(\frac{\Delta z}{L_\varepsilon}\right)$	Discretization of a tail of joint Gaussian PDF
E-const	$\varepsilon_i(\Delta z) = \varepsilon_0/L_\varepsilon$	As in Control
E-uni	$\varepsilon_i(\Delta z) = \mathscr{U}(0, 2\varepsilon_0/L_\varepsilon)$	As in Control
Srf-stoch	As in Control	Stochastically drawn from the tail of joint Gaussian PDF
Srf-const	As in Control	Constant for all updrafts; computed from integral over the tail of Gaussian PDF
E-Srf-const	$\varepsilon_i(\Delta z) = \varepsilon_0/L_\varepsilon$	Constant for all updrafts; computed from integral over the tail of Gaussian PDF
Diag	As in Control	As in Control
Profiles of mean variables kept constant		

two parameterizations are modified in several different ways. Table 1 lists all the experiments and briefly describes these modifications. The Control experiment is our reference from the previous section. In the E-const experiment, the entrainment rate is constant, and in the E-uni experiment, it is drawn from a uniform distribution instead of a Poisson distribution. The Srf-stoch experiment differs from the Control in the way the surface updraft properties are defined. In this experiment, the surface updraft thermodynamic properties are randomly sampled such that the probabilities of their values are proportional to the tail of the joint PDF, and the surface updraft area is the same for all updrafts. In the Srf-const experiment, surface conditions are constant and the same for all updrafts. The E-Srf-const experiment combines the E-const and Srf-const using constant entrainment rates and surface conditions for all updrafts. Since all updrafts have the same properties, this experiment is equivalent to a single bulk mass-flux model with a constant fractional updraft area. Finally, in the Diag experiment, all prognostic variables are fixed in time, and the EDMF parameterization is used only for diagnostic purposes. In this experiment, the EDMF parameterization is identical to the Control experiment. All the modified experiments are designed such that the entrainment rate averaged over the updrafts and vertical levels equals $\langle\varepsilon\rangle = \varepsilon_0/L_\varepsilon$, which is the same as in the Control experiment, and the mean updraft surface conditions are always equal to the ones from the Control experiment.

Figure 6 shows CC and LWP as the functions of the surface UA, for the sensitivity experiments. In the Diag experiment, in which convection does not interact with the mean fields, the CC and LWP are almost proportional to the surface UA. In fact, in this experiment, almost all updrafts condense at the cloud base and reach similar heights (not shown). These results highlight the importance of interactions between convection and mean fields (cf. Neggers et al. 2006; van Stratum et al. 2014; Neggers 2015).

In all other sensitivity experiments, the dependence of CC and LWP on the surface UA falls into two regimes, which are separated by what we define as a critical surface UA (UAc). For surface UAs smaller than UAc, the CC and LWP are approximately proportional to the surface UA. When the surface UA surpasses UAc, both LWP and CC tend to saturate and either stay fairly constant or even decrease with a further increase of the surface UA. The value of UAc varies among the experiments from less than 5% to around 20%. Figure 6 shows that experiments are characterized by a smaller UAc better agree with the LES results for a large range of surface UAs. The key result from Fig. 6 is that UAc is primarily controlled by the parameterization of the entrainment rate and only marginally depends on the parameterization of surface updraft conditions, indicating that entrainment plays a more significant role in determining the spread in the updraft properties. This can be seen from the small differences in UAc among the Control, Srf-const and Srf-stoch experiments. In the experiments with constant entrainment rates (i.e., E-const and E-Srf-const), UAc grows to significantly larger values that are out of the LES range. The differences in UAc between these two experiments show that for a constant entrainment rate, variability among the updraft surface conditions marginally improves the model sensitivity to surface UA. It is interesting to note that in the E-uni experiment, UAc is larger than in the Control experiment. This is likely associated with the fact that the variability of the vertically integrated uniform distribution is smaller than the variability of the Poisson distribution, which results in a smaller spread of the plume ensemble in the E-uni experiment.

To better understand the representation of convection in the two most different experiments, Figs. 7a and 7b show time series of the cloud-top height

Brought to you by NOAA Central Library | Unauthenticated | Downloaded 03/07/22 07:40 PM UTC

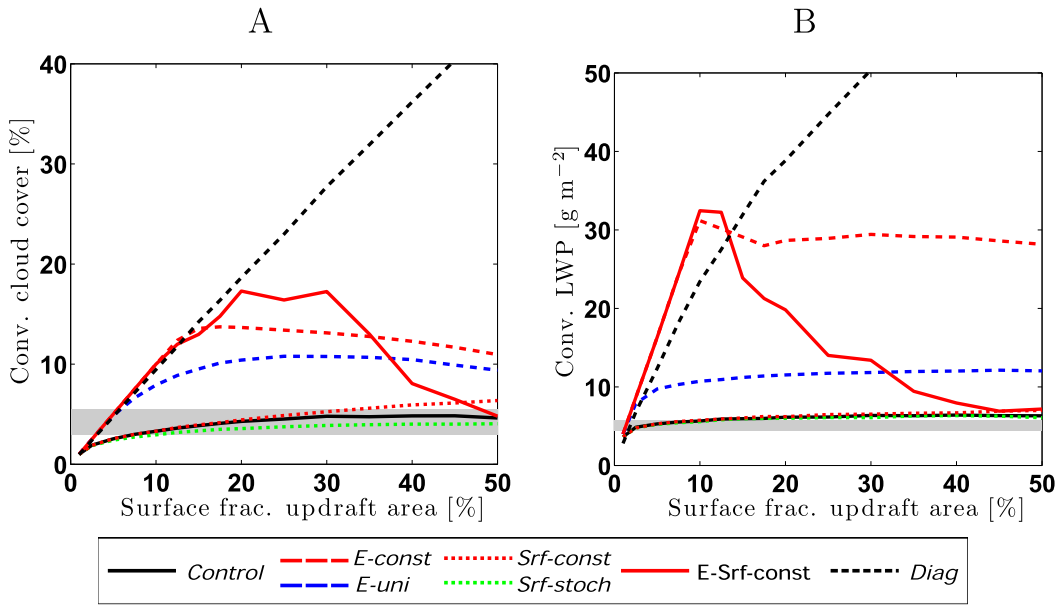

FIG. 6. (a) Cloud cover and (b) liquid water path as a function of surface UA for a set of modified experiments as listed in the legend (see Table 1 for a detailed description). The gray shading represents the envelopes of LES results spanning the second and the third quartiles. All the results are averaged from the second through the sixth simulation hours.

for different surface UAs from the Control and E-Srf-const experiments. Figure 7a shows that in the Control experiment, cloud-top height stays fairly constant in time, and it is virtually independent of the surface UA. In contrast, in the E-Srf-const experiment, temporal changes in the cloud-top height are significant (Fig. 7b). As the surface UA exceeds around 15% (which is close to UAc for this experiment), convection transitions from a steady-state regime to an intermittent regime. For the intermittent regime, periods of more developed convection are followed by periods of suppressed convection. As the surface UA further increases, periods of shallower convection become even longer. It is important to mention that the intermittency of convection as represented by the E-Srf-const experiment appears to be unrealistic. The results from other experiments (not shown) roughly fall into two categories: all the experiments with entrainment rates taken from the Poisson distribution are similar to the Control experiment, while the behavior of convection in the experiments with deterministic entrainment rates is similar to the E-Srf-const experiment.

Figures 7c and 7d show time series of the cloud-top height and the corresponding convective inhibition (CIN) for the Control and E-Srf-const experiments in which the surface UA is set to 16%. CIN is used as a measure of the barrier that the updrafts need to overcome before reaching the cloud layer and has earlier been identified to control the cloud-base convective properties (e.g., Neggers 2015). For the Control simulation, the CIN and the depth of convective clouds are both reasonably constant. For the E-Srf-const experiment, the low-frequency variability of CIN is linked with the development cycle of convective clouds. When moist convection sets in, it overly stabilizes the subcloud layer (seen as more negative CIN), which then prevents its subsequent formation. When moist convection is absent, the large-scale forcing gradually reduces CIN. It eventually leads to the development of very shallow and then deeper moist convection, which again overly stabilizes the subcloud layer and terminates itself. This low-frequency intermittency of convection in E-Srf-const does not represent any physical process and is purely a result of the plume model formulation. The duration of convective and convection-free periods is a strong function of the prescribed surface UA, with shorter cloud formation periods for larger UA.

The two analyzed experiments yield significantly different quasi-equilibrium states of convection (in terms of CIN and CC) owing to the mentioned differences in the updraft properties. The near-surface conditions and entrainment rates vary among the updrafts for Control, while they are all the same for E-Srf-const. As a consequence, the weaker updrafts in Control terminate at lower levels than in E-Srf-const, and the

Brought to you by NOAA Central Library | Unauthenticated | Downloaded 03/07/22 07:40 PM UTC

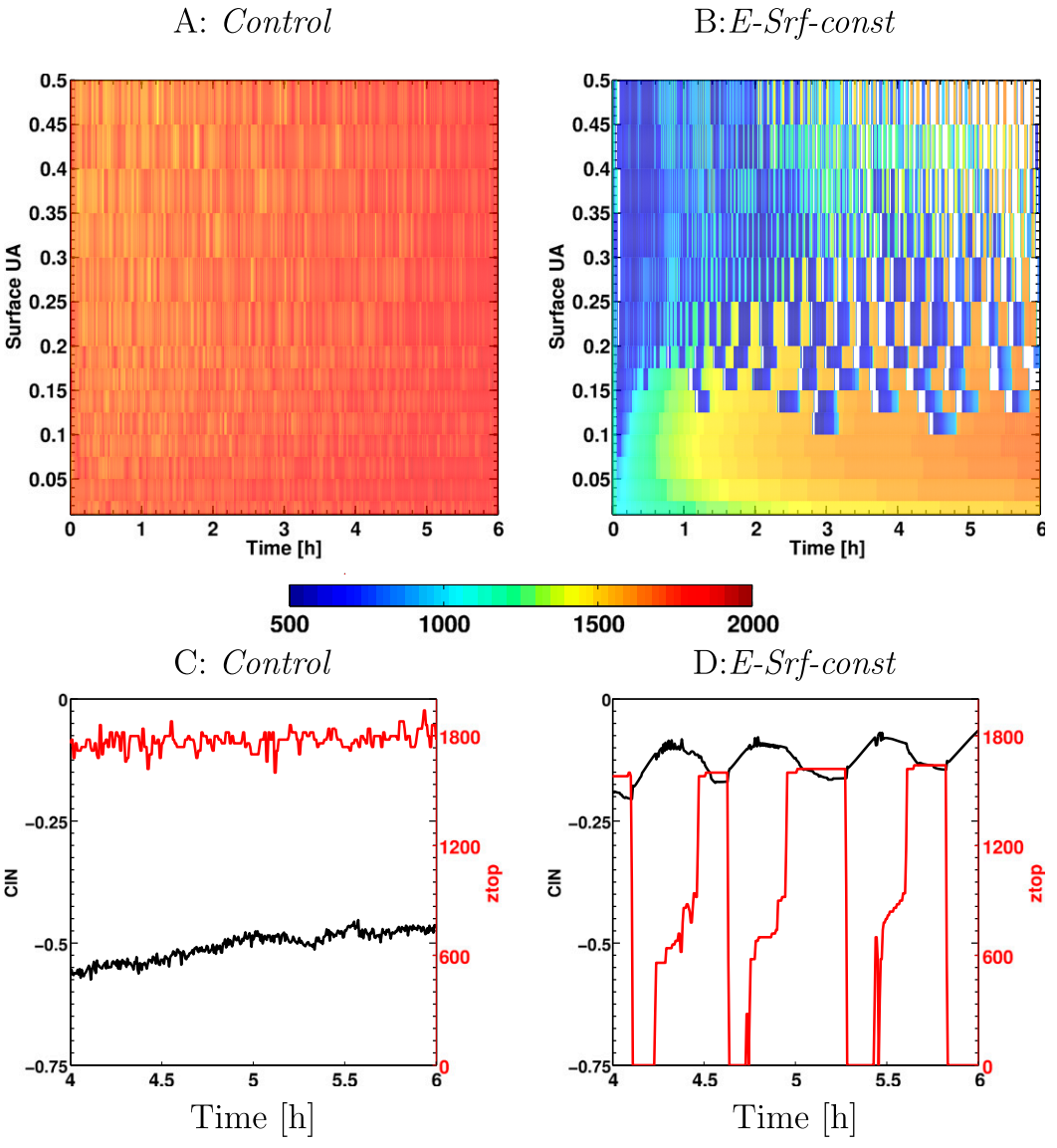

FIG. 7. (top) Time evolution of the cloud-top height (colors) for a set of surface UAs from two different EDMF experiments: (a) Control and (b) E-Srf-const. Each horizontal sequence of colored stripes represents one simulation with the surface UA as indicated on the vertical axis. White patches represent the lack of convective clouds. (bottom) Time series of cloud-top height and convective inhibition over the last two hours of simulation for experiments with surface UA of 16%: (c) Control and (d) E-Srf-const experiments.

remaining updrafts are more buoyant compared those for E-Srf-const. Therefore, they can overcome larger negative values of CIN. All updrafts in the E-Srf-const experiment have the same properties, and they terminate at the same vertical level.

d. A two-layer model for steady-state convection

To highlight the role of interactions between the mean fields and convection, and to find a physical correlate of UAc, described in the previous section, we design a simple two-layer model for steady-state convection. The two layers considered are the well-mixed dry subcloud layer and the moist convective layer aloft. The two-layer model is used to find the properties of convective updrafts for a given state of the atmosphere under the approximation that convection is in equilibrium with the large-scale forcing.

1) SUBCLOUD LAYER

In the subcloud layer, convection is represented by a bulk dry updraft extending from the surface to the cloud base. The updraft area and the entrainment rate are

Brought to you by NOAA Central Library | Unauthenticated | Downloaded 03/07/22 07:40 PM UTC

both prescribed to be constant. The grid-mean virtual potential temperature is assumed to be well mixed (i.e., $\partial\overline{\theta}_v/\partial z = 0$). Since virtual potential temperature is, in the absence of condensation, approximately a linear function of the moist conserved variables ($\theta_v \approx \theta_l + \varepsilon\theta_0 q_t$), the updraft equations without the source term [Eq. (A12)] are valid for the virtual potential temperature as well. The values of the updraft potential temperature and vertical velocity at any height in the subcloud layer ($z \le z_{\rm dry}$) are obtained by integrating the updraft equations [Eqs. (A12) and (A14)] from the surface up to the height z. This yields

$$\theta_{v,1}(z) = \overline{\theta}_v + (\theta_{v,1}|_s - \overline{\theta}_v)e^{-\varepsilon z} \tag{14}$$

and

$$w_1(z) = \frac{e^{-b_w\varepsilon z}\sqrt{2a_w g\dfrac{\theta_{v,1}|_s - \overline{\theta}_v}{\theta_0}[e^{(2b_w-1)\varepsilon z} - 1] + \varepsilon(2b_w - 1)w_1^2|_s}}{\sqrt{\varepsilon(2b_w - 1)}}, \tag{15}$$

where the overbar represents the grid average and the subscript 1 denotes the (single) bulk updraft (for a complete description of the symbols, see appendix B).

Surface the updraft properties such as the UA, vertical velocity $w_1|_s$, and the excess of virtual potential temperature ($\theta_{v,i} - \overline{\theta}_v$) are computed in the same way as in the EDMF model [see Eqs. (A15)–(A21)] but for a single updraft ($I = 1$) and are essentially functions of the surface UA.

2) CLOUD LAYER

In the cloud layer, convection is still represented by a single updraft, but its fractional area, unlike in the subcloud layer, can change with height. We assume that the total subgrid flux of virtual potential temperature is well represented by the mass-flux component in this layer, which is in balance with the large-scale forcing, and that the excess of potential temperature in the updrafts with respect to the environment ($\Delta\theta_v^{\rm cld} \equiv \overline{\theta}_{v,1} - \overline{\theta}_v$) is independent of height. The last assumption holds for most of the cloud layer (for the layer between approximately 700 and 1500 m; cf. Fig. 1f). The physical reasoning behind this assumption is the buoyancy sorting mechanism (e.g., Raymond and Blyth 1986). At each model level, the updrafts that are weakly or negatively buoyant terminate, and the remaining subset of active updrafts preserves positive buoyancy. This assumption is only partially correct at the top of the cloud layer, where the updrafts overshoot their neutral buoyancy level, but it helps to simplify the model. Neglecting the vertical derivative of density, the prognostic equation for $\overline{\theta}_v$ can be written as [see Eq. (1)]

$$\frac{\partial\overline{\theta}_v}{\partial t} = -\frac{\partial}{\partial z}\overline{w'\theta'_v} + \overline{S}_{\theta_v} - \sum_{k=1}^{3}\overline{u}_k\frac{\partial\overline{\theta}_v}{\partial x_k}, \tag{16}$$

where the last two terms in Eq. (16) represent the sum of the prescribed source and advection terms for $\overline{\theta}_v$. Neglecting the time derivative in Eq. (16) (because of the steady-state assumption) and integrating Eq. (16) from height $z > z_{\rm dry}$ to $z_{\rm top}$, we get

$$\overline{w'\theta'_v}|_z = -\int_z^{z_{\rm top}}\left(\overline{S}_{\theta_v} - \sum_{k=1}^{3}\overline{u}_k\frac{\partial\overline{\theta}_v}{\partial x_k}\right)dz, \tag{17}$$

where we used the fact that all subgrid fluxes must vanish at $z_{\rm top}$. The subgrid flux at a height z can be written using the mass-flux model as

$$\overline{w'\theta'_v} = a_1 w_1(\theta_{v,1} - \overline{\theta}_v). \tag{18}$$

Combining Eqs. (17) and (18) yields the expression for the provisional value of the height-dependent UA:

$$a_1^p(z) = -\frac{\displaystyle\int_z^{z_{\rm top}}\left(\overline{S}_{\theta_v} - \sum_{k=1}^{3}\overline{u}_k\frac{\partial\overline{\theta}_v}{\partial x_k}\right)dz}{w_1(z)\Delta\theta_v^{\rm cld}}. \tag{19}$$

Because the UA cannot exceed its value at the surface, the UA in the SCM is limited by

$$a_1(z) = \min(a_1^p, a_1|_s). \tag{20}$$

To obtain the vertical profile of updraft velocity, we integrate the velocity equation [Eq. (A14)] from $z_{\rm cld}$ to z with (assumed) constant buoyancy:

$$B_1 = g\Delta\theta_v^{\rm cld}/\theta_0, \tag{21}$$

which yields

$$w_1(z) = \sqrt{\frac{a_w B_1 + [b_w\varepsilon w_1^2(z_{\rm dry}) - a_w B]e^{-2b_w\varepsilon(z - z_{\rm dry})}}{b_w\varepsilon}} \quad \text{for} \quad z_{\rm dry} \le z \le z_{\rm top}. \tag{22}$$

Brought to you by NOAA Central Library | Unauthenticated | Downloaded 03/07/22 07:40 PM UTC

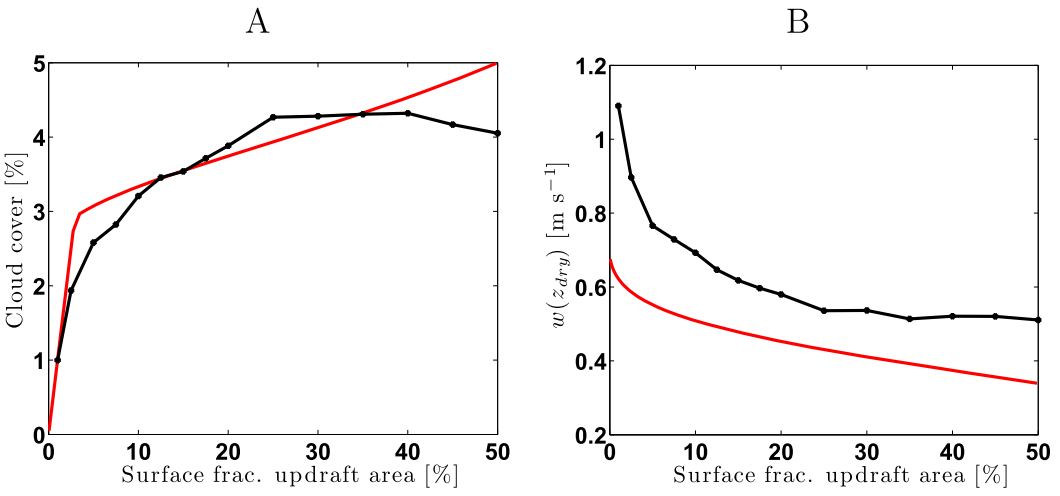

FIG. 8. Comparison of the two-layer model result for $\Delta\theta_v^{\mathrm{cld}} = 0.4$ K with the Control EDMF results. (a) Cloud cover and (b) the cloud-base vertical velocity as a function of surface UA are plotted. Red lines denote the results from the two-layer model. Black lines indicate the Control EDMF results averaged from the second through the sixth simulation hours.

For the conditions at the cloud base, we simply assume that the moist updraft vertical velocity from Eq. (22) and dry updraft vertical velocity from Eq. (15) are equal.

SOLUTION FOR THE BOMEX CASE AND DISCUSSION OF THE RESULTS

To find a solution of the two-layer model for the BOMEX case, we use the same profiles of θ_v and advective and radiative forcing as for the EDMF model simulations. The entrainment rate is set to $\varepsilon = 2.5 \times 10^{-3}\,\mathrm{m}^{-1}$, which is close to the mean value used by the EDMF model. The cloud base and cloud top are fixed at 600 and 2000 m, respectively, which correspond to the levels obtained in the previous experiments. We first chose $\Delta\theta_v^{\mathrm{cld}} = 0.4$ K [Eq. (21)] and compared the results against the Control EDMF simulation. This value was found to bring the results from the two-layer model close to those from the EDMF model and facilitate the comparison. Additionally, we calculated the updraft properties for a range of $\Delta\theta_v^{\mathrm{cld}}$ and compared them against the results from the EDMF sensitivity experiments.

Figures 8a and 8b show CC and vertical velocity at the cloud base as the functions of the surface UA from the two-layer model (for $\Delta\theta_v^{\mathrm{cld}} = 0.4$ K) and from the EDMF Control experiment. The two-layer model produces two distinct regimes for CC, similarly to the (Control) EDMF model, with the UAc around 3%. When the surface UA is lower than UAc, cloud cover equals the surface UA. For the surface UA greater than UAc, cloud cover only slightly increases, in agreement with the reference results. In the subcritical regime, even though all convective updrafts condense, they are still too narrow to provide enough subgrid transport needed to compensate for the destabilization by the large-scale component [i.e., $a_1|_s$ in Eq. (20) is smaller than a_1^p]. When the surface UA is greater than UAc, the CC only weakly depends on the surface UA. This dependence results from the fact that for an increased surface UA, a wider portion of the tail of the near-surface PDF of vertical velocity (and buoyancy) is represented by the bulk updraft. Consequently, these two parameters have to decrease somewhat as they reflect mean updraft properties from the tail. Reducing the buoyancy and vertical velocity at the surface results in lower values of these properties at the cloud base as well. To satisfy the steady-state equation for the mean virtual potential temperature [Eq. (19)], this deficit in the buoyancy and vertical velocity at the cloud base needs to be compensated by an increased CC, which we see in the solution. The cloud-base vertical velocity from the EDMF tends to be somewhat larger than from the two-layer model. This is because EDMF allows weaker updrafts to terminate before reaching the cloud base, which is not represented by the single bulk updraft in the two-layer model. Overall, the transition between the two CC regimes occurs for the surface UA at which the equilibrium between large-scale forcing and convection is achieved.

The question remains why UAc differs among the EDMF experiments. Assuming that the cloud base and the cloud top, as well as the profile of grid-mean virtual potential temperature, are the same for all experiments, the two-layer model suggests that the only differences among the experiments regard the buoyancy of moist updrafts (i.e., $\Delta\theta_v^{\mathrm{cld}}$). Figure 9a shows the dependence of

Brought to you by NOAA Central Library | Unauthenticated | Downloaded 03/07/22 07:40 PM UTC

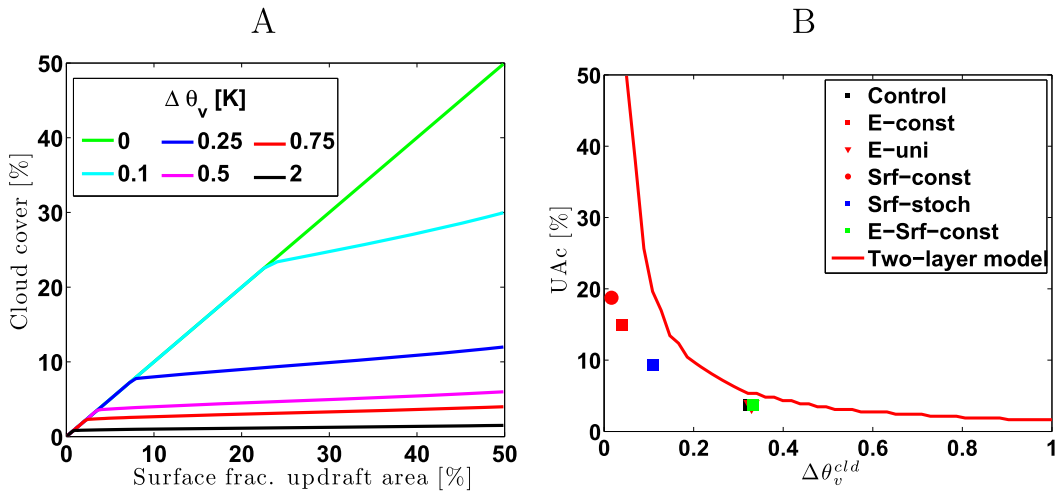

FIG. 9. (a) Cloud cover as a function of the surface UA for a set of $\Delta\theta_v|_{\text{cld}}$ from the two-layer model and (b) critical surface UA as a function of $\Delta\theta_v$ in the two-layer model (red line) and the modified EDMF simulations (as described in the legend). The UAc was computed as the value of the surface UA at which it exceeds the moist UA by 2%, and $\Delta\theta_v$ is the mean updraft virtual potential temperature in the cloud layer between 700 and 1200 m.

CC on the surface UA in the two-layer model for a range of $\Delta\theta_v^{\text{cld}}$. As before, a linear correlation between CC and UA occurs when the surface UA is smaller than UAc, and CC only marginally increases for larger UAs. The results also show a strong dependence of UAc on $\Delta\theta_v^{\text{cld}}$. Figure 9b depicts UAc as a function of $\Delta\theta_v^{\text{cld}}$ for the BOMEX case in the two-layer model and in the modified EDMF experiments. In the two-layer model, the relationship between UAc and $\Delta\theta_v^{\text{cld}}$ is inversely proportional, with a strongly similar behavior to that seen in the modified experiments. This correlation confirms that most of the differences between the EDMF experiments are a consequence of the differences in the mean virtual potential temperature within the updrafts. The differences in the virtual potential temperature can be related to the representation of the spread of thermodynamic variables among convective plumes.

4. Summary and conclusions

In this work, we investigate the role of the underlying physical mechanisms controlling the subgrid transport in EDMF models for a benchmark case of marine shallow convection. To this end, we improve on the formulation of the stochastic multiplume EDMF model of Sušelj et al. (2013). Specifically, the model no longer assumes that the thermodynamic and kinematic properties of the nonconvective environment equal their grid-mean values. Consequently, a new term appears in the final expression of the subgrid fluxes representing the subsiding environment, which is typically neglected in other EDMF models. A large part of this work investigates the features of multiplume convective transport. An advantage of the multiplume approach is the ability to more explicitly capture the nonlinear interactions between the different plumes and the environment. However, the variability of thermodynamic and kinematic properties for the ensemble of updrafts needs to be properly represented. Recent studies suggest two mechanisms responsible for this spread, namely, different surface updraft conditions (e.g., Cheinet 2003; Neggers et al. 2009) or the lateral turbulent entrainment between the updrafts and the environment in which they grow (e.g., Romps and Kuang 2010; Brast et al. 2016), without a consensus as to which of these two is more important. Our model combines the two approaches as the simulated convective plumes differ because of both varying surface conditions and lateral entrainment. To understand the relative importance of these two components, we examine how they shape the termination heights of individual updrafts. We also design a set of modified EDMF experiments in which the representation of these two components is simplified. To better understand the role of the coupling between the mean fields and convection, we design a two-layer model for steady-state convection.

Although this manuscript is focused on the BOMEX subtropical shallow-convection case, this latest version of EDMF has been validated for a variety of other case studies, including (i) the growth of a dry convective boundary layer, first suggested by Nieuwstadt et al. (1992) and (ii) the diurnal cycle of shallow nonprecipitating convection over land—the ARM case of Brown et al. (2002). These results are not shown in the

Brought to you by NOAA Central Library | Unauthenticated | Downloaded 03/07/22 07:40 PM UTC

current paper but do confirm the accuracy of this new EDMF version in realistically depicting the behavior of atmospheric boundary layer turbulence and shallow moist convection for a variety of situations. Results from the EDMF model compare well with the LES results for a range of prescribed surface updraft areas (UAs) as long as the surface UA is higher than around 5%. The model reproduces the mean thermodynamic fields and essential features of moist updrafts well, including the updraft fractional area, vertical velocity, temperature, and moisture. This result is particularly encouraging as it is not apparent what values of surface UA should be used in a parameterization. In some EDMF models, surface UA is prescribed, although it can differ significantly from model to model (e.g., Soares et al. 2004; Sušelj et al. 2013), while in others, it is parameterized (e.g., Pergaud et al. 2009). In the simulations with large surface UA, the term representing the mass flux due to the subsiding environment becomes significant in the subcloud layer. Although our results show a lack of sensitivity to the surface updraft area, our previous work (and other studies) leads us to conclude that it is more physically appropriate to represent small-scale turbulent motions using an eddy-diffusivity formulation. In addition, recent studies (e.g., Couvreux et al. 2010) indicate that convective plumes cover between 10% and 30% of the fractional area in the surface layer. Therefore, even though this version of the EDMF parameterization is relatively insensitive to the surface UA, we suggest the utilization of values of surface UA between 10% and 30%.

We find that around the cloud base, both the surface conditions and the lateral entrainment determine which of the updrafts terminate. If the updraft reaches the condensation level, its termination height becomes essentially dependent on the lateral entrainment.

Results from the sensitivity experiments indicate that interactions between convection and the mean fields are crucial for shaping updraft properties. In fact, the low sensitivity of the time-averaged convective properties to the surface UA is primarily a consequence of these interactions. In simulations in which convection is coupled to the mean field, the dependence of the total moist updraft area (CC) on the surface UA falls into two regimes. For surface UAs smaller than some critical updraft area (UAc), the CC is proportional to the surface UA. Once the surface UA increases above UAc, the CC saturates. The results of the two-layer model explain this dependence. For small surface UAs, convection is too weak to counterbalance the large-scale forcing. In this regime, virtually all updrafts condense at the cloud base, and therefore, cloud cover is similar to UA. For larger surface UAs, cloud cover also increases until UAc is reached. The UAc is the minimum value of surface UA at which convective tendencies balance the (prescribed) large-scale forcing. For a supercritical UA, sufficient transport is provided by a fraction of updrafts, and thus, cloud cover is smaller than the surface UA.

We show that the variability among convective updrafts is controlled by stochastic entrainment, which is critical for a realistic representation of moist convection. In particular, two main features strongly depend on this variability. First, the value of UAc is larger in simulations with smaller variability, and the results are less consistent with LES. Second, reducing the updraft variability yields intermittent moist convection on larger time scales. Using a stochastic entrainment rate formulation improves these two issues.

In this work, convection is modeled with 100 updrafts per time step, each with its own surface conditions and profile of entrainment rates. We show that this number can be significantly smaller although at the expense of increased intermittency of convective properties. In future work, we will investigate how to prescribe a number of updrafts to mimic the stochastic nature of convection and its resolution dependence, which becomes essential in the convective gray zone (e.g., Sakradzija et al. 2015; Kurowski and Teixeira 2018) and plays a key role in ensemble weather prediction (Buizza et al. 1999; Lin and Neelin 2000; Teixeira and Reynolds 2008). For the convective gray zone problem, we will build on the work of Brast et al. (2018).

Acknowledgments. The research was carried out at the Jet Propulsion Laboratory, California Institute of Technology, under a contract with the National Aeronautics and Space Administration. Parts of this research were supported by the U.S. Department of Energy, Office of Biological and Environmental Research, Earth System Modeling; the NASA MAP Program; the Office of Naval Research, Marine Meteorology Program; and the NOAA/CPO MAPP Program. We thank Wayne Angevine and two anonymous reviewers for constructive comments. We also thank Bridget Samuels for proofreading the manuscript.

APPENDIX A

Description of the EDMF Parameterization

a. Parameterization of subgrid-scale mixing in the nonconvective environment

An important consequence of the EDMF decomposition is that the environment represents a subgrid-scale domain devoid of convective plumes. Therefore, the

Brought to you by NOAA Central Library | Unauthenticated | Downloaded 03/07/22 07:40 PM UTC

subgrid scale in the environment can be well represented with a local downgradient approximation [Eq. (6)]. The parameterization requires a model for $K_{h/m,e}$, which is a short notation for the eddy-diffusivity ($K_{h,e}$) or eddy-viscosity ($K_{m,e}$) coefficients in the environment.[A1] These coefficients are parameterized as a product of the diagnostic turbulent length scale and velocity scale in the environment where the velocity scale is represented by the square root of environmental TKE (e_e):

$$K_{h/m,e} = l_{h/m,e}\sqrt{e_e}, \tag{A1}$$

with a similar notation as above used for the corresponding length scales. As detailed below, the model distinguishes between the environmental and the grid-mean TKE. The EDMF model solves the prognostic equation for the grid-mean TKE and diagnoses the environmental TKE.

1) TKE EQUATION

The grid-mean TKE (e) is computed using a well-known prognostic equation (e.g., Stull 1988):

$$\frac{\partial e}{\partial t} = -\sum_{k=1}^{3}\overline{u}^k\frac{\partial e}{\partial x^k} - \frac{1}{\rho}\frac{\partial}{\partial z}\rho\overline{w'e'} - \overline{w'u'}\frac{\partial \overline{u}}{\partial z} - \overline{w'v'}\frac{\partial \overline{v}}{\partial z} + \frac{g}{\theta_0}\overline{w'\theta_v'} - c_\varepsilon\frac{e^{3/2}}{l_\varepsilon}, \tag{A2}$$

where the first two terms on the rhs represent the resolved and the subgrid-scale transport (where the summation is over the two horizontal and one vertical direction), the third and fourth terms are the shear production/consumption of TKE, the fifth term is the buoyancy production/consumption, and the last term represents dissipation.

Subgrid fluxes in the shear- and buoyancy-related source terms are computed with the EDMF approximation [Eq. (5)], and $c_\varepsilon = 0.16$ is constant. In the current model version, the subgrid transport of TKE is modeled with a simple eddy-diffusivity approach:

$$\overline{w'e'} = -K_{m,e}\frac{\partial e}{\partial z}. \tag{A3}$$

Recalling that the total TKE is defined as $e = (1/2)\sum_{k=1}^{3}\overline{u_k'u_k'}$ and environmental TKE as $e_e = (1/2)\sum_{k=1}^{3}\overline{u_k'u_k'}|_e$ (where u_k represents the velocity components along the three k directions), the EDMF decomposition in Eq. (4) together with the assumption of horizontally homogeneous updrafts is used to write the total TKE as a sum of the three components. The environmental TKE can be expressed as

$$e_e = \frac{e}{a_e} - \frac{1}{2}\sum_{k=1}^{3}(u_e^k - \overline{u}^k) - \frac{1}{2}\sum_{i=1}^{I}\sum_{k=1}^{3}\frac{a_i}{a_e}(u_i^k - \overline{u}^k)^2. \tag{A4}$$

2) TURBULENT LENGTH SCALES

Specification of the turbulent length scales for the eddy-diffusivity, eddy-viscosity, and dissipation terms is one of the most uncertain parts of the EDMF model. Over the past decades, many expressions for those length scales were proposed. Here, we follow the approach of Teixeira and Cheinet (2004) to define master length scale $l_{0,e}$ for diffusion and dissipation:

$$l_{0,e} = \tau_e\sqrt{e_e} + (kz - \tau_e\sqrt{e_e})e^{-z/z_{\rm sf}}, \tag{A5}$$

where $z_{\rm sf} = 100$ m is assumed to be the surface-layer depth. The length scale $l_{0,e}$ is defined in a way to converge to the Prandtl mixing length kz close to the surface and to the TKE-dependent length scale $\tau_e\sqrt{e_e}$ far above the surface. The time scale τ_e is defined as

$$\tau_e^{-1} = \begin{cases} (\tau_0^{-1} + 0.75N_e)^{-1} & \text{for} \quad N_e^2 > 0 \\ \tau_0^{-1} & \text{for} \quad N_e^2 \le 0, \end{cases} \tag{A6}$$

where N_e is a Brunt–Väisälä frequency for the environment and τ_e is a combination of the time scale for neutral (τ_0) and stable [$1/(0.75N_e)$] layers. The time scale for neutral atmosphere is modeled as

$$\tau_0 = \frac{1}{3}\frac{z_{\rm dry}}{\sqrt{w_*^2 + u_*^2}}, \tag{A7}$$

where $z_{\rm dry}$ is the depth of dry (subcloud) layer and w_* and u_* are the convective and friction surface velocity scales, respectively (see appendix B for its definition). The viscosity and diffusivity length scales are computed as

$$l_{m,e} = l_{0,e}\alpha_m({\rm Ri}_e) \tag{A8}$$

and

$$l_{h,e} = l_{0,e}\alpha_h({\rm Ri}_e), \tag{A9}$$

where α_h and α_m are the stability functions that follow the quasi-normal scale elimination theory (Sukoriansky et al. 2005, 2006). They depend on the environmental bulk Richardson number ($\rm Ri_e$):

[A1] The eddy diffusivity coefficient is used as a mixing coefficient for thermodynamic variables (θ_l, q_t), and the eddy-viscosity coefficient is used for the wind speed components u and v and TKE.

Brought to you by NOAA Central Library | Unauthenticated | Downloaded 03/07/22 07:40 PM UTC

$$\alpha_m = \begin{cases} \dfrac{1 + 8\mathrm{Ri}_e^2}{1 + 2.3\mathrm{Ri}_e + 35\mathrm{Ri}_e^2} & \text{if} \quad \mathrm{Ri}_e > 0 \\ 1 & \text{if} \quad \mathrm{Ri}_e \le 0 \end{cases}$$

and

$$\alpha_h = \begin{cases} \dfrac{1.4 - 0.001\mathrm{Ri}_e + 1.29\mathrm{Ri}_e^2}{1 + 2.3\mathrm{Ri}_e + 19.81\mathrm{Ri}_e^2} & \text{if} \quad \mathrm{Ri}_e > 0 \\ 1.4 & \text{if} \quad \mathrm{Ri}_e \le 0. \end{cases}$$

Note that in the above parameterization, the turbulent Prandtl number ($\mathrm{Pr}_e = K_{m,e}/K_{h,e} = l_{m,e}/l_{h,e}$) is a function of Ri_e. For unstable and neutral layers ($\mathrm{Ri}_e \le 0$), the turbulent Prandtl number equals $1/1.4 \approx 0.71$, and for stably stratified layers with very large Ri_e ($\mathrm{Ri}_e \to \infty$), it approaches 3.5.

The dissipative length scale is parameterized in a similar manner as the eddy-diffusivity/viscosity length scales but is the function of the grid-mean TKE:

$$l_\varepsilon = l_{\varepsilon_0} + \left(kz - l_{\varepsilon_0}\right) e^{-z/z_{\mathrm{sf}}}, \tag{A10}$$

with l_{ε_0} following Mellor and Yamada (1982):

$$l_{\varepsilon_0} = 0.12 \frac{\int_0^\infty z\sqrt{e}\, dz}{\int_0^\infty \sqrt{e}\, dz}. \tag{A11}$$

b. Convective mass-flux parameterization

The mass-flux scheme is designed to represent an ensemble of steady-state laterally entraining updrafts originating at the surface with the multiplume model. The plumes can remain dry or condense, which depends on the difference between their total and saturated water mixing ratios. In the current model, the plumes represent shallow convection and therefore do not include parameterization of any microphysical processes. The horizontal area of the individual plume is constant from the surface to its termination height.

A steady-state equation for variables $\varphi_i = \{\theta_{li}, q_{ti}, u_i, v_i, w_i\}$ in the ith plume can be written as

$$\frac{\partial \varphi_i}{\partial z} = \varepsilon_i(\overline{\varphi} - \varphi_i) + \frac{S_{\varphi,i}}{w_i}, \tag{A12}$$

where ε_i represents the entrainment rate, $S_{\varphi,i}$ the source term of φ, and w_i the mean vertical velocity of the ith plume. In this model, we assume that the ith plume entrains properties of the grid-mean field, which implicitly assumes interaction between convective plumes. Namely, the entrained air originates from both an ensemble of convective plumes and the environment, where the fraction of the entrained air from each of these components is equal to the fractional area of the corresponding component. One could formulate a plume model in which the plumes entrain the environmental air by replacing $\overline{\varphi}$ with φ_e in Eq. (A12). In that parameterization, one would assume that the plumes are noninteractive, which is probably less realistic, especially when the total updraft fractional area approaches unity.

The plume's thermodynamic variables (θ_{li} and q_{ti}) are conserved during condensation; therefore, their respective source terms are zero. Source terms for the horizontal momentum are modeled following Romps (2012), who showed that they effectively decrease the entrainment rate by a factor of 3. Therefore, the source term for the u component of horizontal momentum reads as

$$S_{u,i} = -\frac{2}{3}\varepsilon_i w_i(\overline{u} - u_i), \tag{A13}$$

and the equivalent equation is used to parameterize the source term for the v component. Vertical velocity source terms are parameterized following de Roode et al. (2012), and the final equation for the vertical velocity is

$$\frac{1}{2}\frac{\partial w_i^2}{\partial z} = a_w B_i - b_w \varepsilon_i w_i^2, \tag{A14}$$

where $B_i = g(\theta_{v,i}/\overline{\theta}_v - 1)$ is the buoyancy of the ith plume with respect to the grid mean, and $a_w = 1$ and $b_w = 1.5$ are constants. Equivalent to entrainment parameterization, the plumes are assumed to interact with the grid-mean buoyancy. The b_w parameter includes the parameterization of the pressure perturbation term and the subplume variability. The vertical velocity equation is different from that used in Sušelj et al. (2012, 2013), but it agrees better with one of the possible parameterizations discussed in de Roode et al. (2012).

Contrary to many parameterization (e.g., Soares et al. 2004; Neggers et al. 2009), in which the horizontal area of plumes evolve in the vertical governed by a steady-state continuity equation (which assumes the balance between the vertical mass flux, entrainment, and detainment rate), we assume that each individual plume has a fixed horizontal area as, for example, in Witek et al. (2011b). A practical consequence of this assumption is that the detrainment rate, for which the

Brought to you by NOAA Central Library | Unauthenticated | Downloaded 03/07/22 07:40 PM UTC

underlying physical processes are poorly understood, does not need to be parameterized. As a result, the total horizontal area of convective plumes cannot increase with height and therefore cannot exceed its surface area.

As mentioned above, the subgrid convection is represented by $i = 1, \ldots, I$ plumes initialized at the surface. Each plume is characterized with different surface conditions and experiences stochastic entrainment rates during its ascent. The equations governing plume properties [Eqs. (A12) and (A14)] are independently integrated for each plume from the surface up to the level where its vertical velocity becomes zero. At that level, the plume terminates. Condensation within a plume occurs when its total water exceeds the saturated mixing ratio [i.e., where $q_{ti} > q_{si}(T_i, p)$]. The resulting convective cloud water is computed as an excess of the total water over the saturated value (i.e., $q_{li} = q_{ti} - q_{si}$).

1) Surface conditions for convective plumes

Surface conditions for convective plumes are parameterized following Cheinet (2003). This parameterization builds on the measurements by Mahrt and Paumier (1984), who show that the near-surface vertical velocity, virtual potential temperature, and total water mixing ratio are to the first approximation normally distributed and positively correlated. Therefore, a normal PDF of the near-surface vertical velocity with zero mean and the standard deviation of σ_w is prescribed [$N(0, \sigma_w)$]. We assume that convective updraft near the surface represent a positive tail of this vertical velocity distribution, with their values ranging from the minimum $w_{\min}$ to the maximum $w_{\max}$ (the latter is prescribed to avoid unrealistically strong plumes). The PDF of vertical velocity is discretized into I bins (with I representing the total number of plumes), where the ith plume accounts for the velocity between $w_{\min,i} = w_{\min} + (i-1)\Delta w$ and $w_{\max,i} = w_{\min} + i\Delta w$, with $\Delta w = (w_{\max} - w_{\min})/I$. The surface area of the ith plume is computed as an integral of the PDF of vertical velocity from $w_{\min,i}$ to $w_{\max,i}$:

$$a_i|_s = \int_{w_{\min,i}}^{w_{\max,i}} N(0,\sigma_w)\, dw = \frac{1}{2}\left[\operatorname{erf}\left(\frac{w_{\max,i}}{\sqrt{2}\sigma_w}\right) - \operatorname{erf}\left(\frac{w_{\min,i}}{\sqrt{2}\sigma_w}\right)\right], \quad \text{(A15)}$$

where the subscript s denotes surface values. In all numerical experiments, we use $w_{\max} = 3\sigma_w$ and investigate sensitivity of the results to the value of $w_{\min}$.

Surface vertical velocity for the ith plume is formulated as

$$w_i|_s = \frac{\int_{w_{\min,i}}^{w_{\max,i}} N(0,\sigma_w) w\, dw}{\int_{w_{\min,i}}^{w_{\max,i}} N(0,\sigma_w)\, dw} = \frac{\sigma_w}{\sqrt{2\pi}} \frac{e^{-w_{\min,i}^2/(2\sigma_w^2)} - e^{-w_{\max,i}^2/(2\sigma_w^2)}}{a_i|_s}. \quad \text{(A16)}$$

Thermodynamic properties of the ith plume (i.e., virtual potential temperature and total water mixing ratio) are obtained assuming that the near-surface vertical velocity, virtual potential temperature, and total water mixing ratio can be represented by the joint normal PDF, where the above-described PDF of vertical velocity is a marginal distribution of this joint PDF. The surface value of virtual potential temperature in the ith plume is computed as

$$\theta_{v,i}|_s = \overline{\theta}_v|_s + c(w,\theta_v) w_i|_s \frac{\sigma_{\theta_v}}{\sigma_w} \quad \text{(A17)}$$

and of total water mixing ratio as

$$q_{t,i}|_s = \overline{q}_t|_s + c(w,q_t) w_i|_s \frac{\sigma_{q_t}}{\sigma_w}, \quad \text{(A18)}$$

where the correlation coefficients between the vertical velocity and corresponding thermodynamic variables are fixed as $c(w, q_t) = c(w, \theta_v) = 0.58$, and are equal to each other, unlike in Cheinet (2003). The variances of vertical velocity σ_w, total water mixing ratio σ_{q_t}, and virtual potential temperature σ_{θ_v} at the surface are parameterized as

$$\sigma_w = 1.34 w_* \left(\frac{z_0}{z_{\text{top}}}\right)^{1/3} \left(1 - 0.8\frac{z_0}{z_{\text{top}}}\right), \quad \text{(A19)}$$

$$\sigma_{q_t} = 1.34 q_* \left(\frac{z_0}{z_{\text{top}}}\right)^{-1/3}, \quad \text{(A20)}$$

and

$$\sigma_{\theta_v} = 1.34 \theta_* \left(\frac{z_0}{z_{\text{top}}}\right)^{-1/3}, \quad \text{(A21)}$$

where z_{top} is the depth of convective layer and $w_* \equiv (g/\theta_v)\overline{w'\theta_v'}|_s z_{\text{top}}$ is the convective velocity. Here, we take $z_0 = 0.1 z_{\text{top}}$, and $q_* = \overline{w'q_t'}|_s / w_*$ and $\theta_* = \overline{w'\theta_v'}|_s / w_*$ are the convective moisture and temperature scales, respectively.

Brought to you by NOAA Central Library | Unauthenticated | Downloaded 03/07/22 07:40 PM UTC

TABLE B1. List of symbols and their description.

Symbol	Description
	General variables
a_i, a_e	Fractional area of the ith updraft and the environment
$c_p = 1.06 \times 10^3\ \mathrm{J\,kg^{-1}\,K^{-1}}$	Specific heat of air at constant pressure
$g = 9.8\ \mathrm{m\,s^{-2}}$	Gravity acceleration
$L_v = 2.5 \times 10^6\ \mathrm{J\,kg^{-1}}$	Latent heat of water
q_l, q_s, q_t, q_v	Liquid, saturated, total, and vapor water mixing ratio
S_φ	Source terms for the variable φ
t	Time
$\{u^1, u^2, u^3\} = \{u, v, w\}$	Wind speed components along the x, y, and z directions
$w_* \equiv \left(\frac{g}{\theta_v}\overline{w'\theta_v'}\big\|_s z_{\mathrm{top}}\right)^{1/3}$	Convective velocity scale
$\{x^1, x^2, x^3\} = \{x, y, z\}$	Zonal, meridional, and vertical directions
z_b	Height of negative buoyancy flux
z_{dry}	Depth of dry convective boundary layer
z_{top}	Depth of convective layer
$\theta_0 = 300\ \mathrm{K}$	Temperature scale
ρ	Density of dry air
φ_s or $\varphi\big\|_s$	Value of the variable φ at the surface
θ, θ_l, θ_v	Potential, liquid water potential, and virtual potential temperature
	Eddy-diffusivity variables
e, e_e	Grid-mean and environmental TKE
$K_{h/m,e}$	Eddy diffusivity or viscosity coefficients for the environment
$l_{h/m,e}$	Eddy diffusivity or viscosity length scales
l_ε, $l_{\varepsilon 0}$	Dissipative length scales
$N = \sqrt{\frac{g}{\theta_0}\frac{\partial\theta_v}{\partial z}}$	Brunt–Väisälä frequency
$\mathrm{Pr} = K_m/K_h$	Turbulent Prandtl number
$\mathrm{Ri} = \frac{g}{\theta_0}\frac{\frac{\partial\overline{\theta}_v}{\partial z}}{\left(\frac{\partial\overline{u}}{\partial z}\right)^2 + \left(\frac{\partial\overline{v}}{\partial z}\right)^2}$	Bulk Richardson number
$z_{\mathrm{sf}} = 100\ \mathrm{m}$	Surface-layer depth
α_H, α_M	Stability functions for eddy diffusivity and viscosity
φ_e or $\varphi\big\|_e$	Mean value of φ in the environment
$\overline{\varphi'\lambda'}\big\|_e$	Covariance of φ and λ in the environment
τ_e, τ_0	Time scales for the parameterization of $l_{h/m,e}$
	Updraft variables
$a_w = 1$, $b_w = 1.5$	Constants for the vertical velocity equation
$c(w, q_t) = 0.58$	Correlation between surface velocity and q_t
$c(w, \theta_v) = 0.58$	Correlation between surface velocity and θ_v
$i = 1, \ldots, I$	Index denoting the number of updrafts
$\mathscr{P}$	Poisson probability function
$q*$, $\theta*$	Surface moisture and temperature scales
$\mathscr{U}(a, b)$	Uniform distribution on interval $[a, b]$
$w_{\min}$, $w_{\max}$	Limits for the vertical velocity discretization
φ_i or $\varphi\big\|_i$	Average φ in the ith updraft
σ_w, σ_{θ_v}, σ_{q_t}	Standard deviation of w, θ_v, and q_t at the surface
τ_ε, L_ε	Entrainment time and length scales
ε, ε_0	Entrainment rates
$\tilde{\varepsilon}$	Normalized integrated entrainment rate

2) ENTRAINMENT RATE

The lateral entrainment is assumed to be a stochastic process, and its parameterization follows Sušelj et al. (2013). For a plume that extends over the distance dz, a probability that a single entrainment event occurs is described by the binomial distribution. Both the probability of the entrainment event and the strength of the entrainment rate are assumed to be height independent. The actual number of entrainment events over a finite distance Δz (which is the

Brought to you by NOAA Central Library | Unauthenticated | Downloaded 03/07/22 07:40 PM UTC

distance between two vertical model levels) thus follow the Poisson distribution as it is a superposition of binomial distributions. The corresponding entrainment rate is parameterized as

$$\varepsilon_i(\Delta z) = \frac{\varepsilon_0}{\Delta z}\mathscr{P}_i\left(\frac{\Delta z}{L_\varepsilon}\right), \tag{A22}$$

where $\varepsilon_i(\Delta z)$ is the entrainment rate for the ith plume over the distance Δz, the length scale L_ε represents the average distance a plume needs to travel to entrain once and is parameterized as a function of the surface convective velocity $L_\varepsilon = \tau_\varepsilon w_*$ where $\tau_\varepsilon = 80$ s, $\varepsilon_0 = 0.2$ is the fractional entrainment rate of a single entrainment event, and $\mathscr{P}(\lambda)$ represents a random number from Poisson distribution with parameter λ. Note that the entrainment rate (and L_ε in particular) is parameterized differently than in our previous work.

APPENDIX B

List of Symbols

A list of symbols and their descriptions is provided in Table B1.

REFERENCES

Angevine, W. M., 2005: An integrated turbulence scheme for boundary layers with shallow cumulus applied to pollutant transport. *J. Appl. Meteor.*, **44**, 1436–1452, https://doi.org/10.1175/JAM2284.1.

Brast, M., R. A. J. Neggers, and T. Heus, 2016: What determines the fate of rising parcels in a heterogeneous environment? *J. Adv. Model. Earth Syst.*, **8**, 1674–1690, https://doi.org/10.1002/2016MS000750.

——, V. Schemann, and R. A. J. Neggers, 2018: Investigating the scale adaptivity of a size-filtered mass flux parameterization in the gray zone of shallow cumulus convection. *J. Atmos. Sci.*, **75**, 1195–1214, https://doi.org/10.1175/JAS-D-17-0231.1.

Brown, A. R., and Coauthors, 2002: Large-eddy simulation of the diurnal cycle of shallow cumulus convection over land. *Quart. J. Roy. Meteor. Soc.*, **128**, 1075–1093, https://doi.org/10.1256/003590002320373210.

Buizza, R., M. Milleer, and T. N. Palmer, 1999: Stochastic representation of model uncertainties in the ECMWF ensemble prediction system. *Quart. J. Roy. Meteor. Soc.*, **125**, 2887–2908, https://doi.org/10.1002/qj.49712556006.

Chatfield, R. B., and R. A. Brost, 1987: A two-stream model of the vertical transport of trace species in the convective boundary layer. *J. Geophys. Res.*, **92**, 13 263–13 276, https://doi.org/10.1029/JD092iD11p13263.

Cheinet, S., 2003: A multiple mass-flux parameterization for the surface-generated convection. Part I: Dry plumes. *J. Atmos. Sci.*, **60**, 2313–2327, https://doi.org/10.1175/1520-0469(2003)060<2313:AMMPFT>2.0.CO;2.

——, 2004: A multiple mass flux parameterization for the surface-generated convection. Part II: Cloudy cores. *J. Atmos. Sci.*, **61**, 1093–1113, https://doi.org/10.1175/1520-0469(2004)061<1093:AMMFPF>2.0.CO;2.

Chinita, M. J., G. Matheou, and J. Teixeira, 2018: A joint probability density-based decomposition of turbulence in the atmospheric boundary layer. *Mon. Wea. Rev.*, **146**, 503–523, https://doi.org/10.1175/MWR-D-17-0166.1.

Couvreux, F., F. Hourdin, and C. Rio, 2010: Resolved versus parametrized boundary-layer plumes. Part I: A parametrization-oriented conditional sampling in large-eddy simulations. *Bound.-Layer Meteor.*, **134**, 441–458, https://doi.org/10.1007/s10546-009-9456-5.

Dawe, J. T., and P. H. Austin, 2012: Statistical analysis of an LES shallow cumulus cloud ensemble using a cloud tracking algorithm. *Atmos. Chem. Phys.*, **12**, 1101–1119, https://doi.org/10.5194/acp-12-1101-2012.

de Roode, S. R., A. P. Siebesma, H. J. J. Jonker, and Y. de Voogd, 2012: Parameterization of the vertical velocity equation for shallow cumulus clouds. *Mon. Wea. Rev.*, **140**, 2424–2436, https://doi.org/10.1175/MWR-D-11-00277.1.

Hourdin, F., F. Couvreux, and L. Menut, 2002: Parameterization of the dry convective boundary layer based on a mass flux representation of thermals. *J. Atmos. Sci.*, **59**, 1105–1123, https://doi.org/10.1175/1520-0469(2002)059<1105:POTDCB>2.0.CO;2.

Jam, A., F. Hourdin, C. Rio, and F. Couvreux, 2013: Resolved versus parametrized boundary-layer plumes. Part III: Derivation of a statistical scheme for cumulus clouds. *Bound.-Layer Meteor.*, **147**, 421–441, https://doi.org/10.1007/s10546-012-9789-3.

Krueger, S. K., C.-W. Su, and P. A. McMurtry, 1997: Modeling entrainment and finescale mixing in cumulus clouds. *J. Atmos. Sci.*, **54**, 2697–2712, https://doi.org/10.1175/1520-0469(1997)054<2697:MEAFMI>2.0.CO;2.

Kurowski, M., and J. Teixeira, 2018: A scale-adaptive turbulent kinetic energy closure for the dry convective boundary layer. *J. Atmos. Sci.*, **75**, 675–690, https://doi.org/10.1175/JAS-D-16-0296.1.

Lappen, C.-L., and D. A. Randall, 2001: Toward a unified parameterization of the boundary layer and moist convection. Part III: Simulations of clear and cloudy convection. *J. Atmos. Sci.*, **58**, 2052–2072, https://doi.org/10.1175/1520-0469(2001)058<2052:TAUPOT>2.0.CO;2.

Lin, J. W.-B., and J. D. Neelin, 2000: Influence of a stochastic moist convective parameterization on tropical climate variability. *Geophys. Res. Lett.*, **27**, 3691–3694, https://doi.org/10.1029/2000GL011964.

Mahrt, L., and J. Paumier, 1984: Heat transport in the atmospheric boundary layer. *J. Atmos. Sci.*, **41**, 3061–3075, https://doi.org/10.1175/1520-0469(1984)041<3061:HTITAB>2.0.CO;2.

Mellor, G., and T. Yamada, 1982: Development of a turbulence closure model for geophysical fluid problems. *Rev. Geophys.*, **20**, 851–875, https://doi.org/10.1029/RG020i004p00851.

Neggers, R. A. J., 2009: A dual mass flux framework for boundary layer convection. Part II: Clouds. *J. Atmos. Sci.*, **66**, 1489–1506, https://doi.org/10.1175/2008JAS2636.1.

——, 2015: Exploring bin-macrophysics models for moist convective transport and clouds. *J. Adv. Model. Earth Syst.*, **7**, 2079–2104, https://doi.org/10.1002/2015MS000502.

——, B. Stevens, and J. Neelin, 2006: A simple equilibrium model for shallow-cumulus-topped mixed layers. *Theor. Comput. Fluid Dyn.*, **20**, 305–322, https://doi.org/10.1007/s00162-006-0030-1.

Brought to you by NOAA Central Library | Unauthenticated | Downloaded 03/07/22 07:40 PM UTC

——, M. Köhler, and A. Beljaars, 2009: A dual mass flux framework for boundary layer convection. Part I: Transport. *J. Atmos. Sci.*, **66**, 1465–1487, https://doi.org/10.1175/2008JAS2635.1.

Nieuwstadt, F. T. M., P. J. Mason, C.-H. Moeng, and U. Schumann, 1992: Large-eddy simulation of the convective boundary layer: A comparison of four codes. *Turbulent Shear Flows 8*, F. Durst et al., Eds., Springer, 343–367.

Pergaud, J., V. Masson, S. Malardel, and F. Couvreux, 2009: A parameterization of dry thermals and shallow cumuli for mesoscale numerical weather prediction. *Bound.-Layer Meteor.*, **132**, 83–106, https://doi.org/10.1007/s10546-009-9388-0.

Raymond, D. J., and A. M. Blyth, 1986: A stochastic mixing model for nonprecipitating cumulus clouds. *J. Atmos. Sci.*, **43**, 2708–2718, https://doi.org/10.1175/1520-0469(1986)043<2708:ASMMFN>2.0.CO;2.

Rio, C., and F. Hourdin, 2008: A thermal plume model for the convective boundary layer: Representation of cumulus clouds. *J. Atmos. Sci.*, **65**, 407–425, https://doi.org/10.1175/2007JAS2256.1.

——, ——, F. Couvreux, and A. Jam, 2010: Resolved versus parametrized boundary-layer plumes. Part II: Continuous formulations of mixing rates for mass-flux schemes. *Bound.-Layer Meteor.*, **135**, 469–483, https://doi.org/10.1007/s10546-010-9478-z.

Romps, D. M., 2010: A direct measure of entrainment. *J. Atmos. Sci.*, **67**, 1908–1927, https://doi.org/10.1175/2010JAS3371.1.

——, 2012: On the equivalence of two schemes for convective momentum transport. *J. Atmos. Sci.*, **69**, 3491–3500, https://doi.org/10.1175/JAS-D-12-068.1.

——, and Z. Kuang, 2010: Nature versus nurture in shallow convection. *J. Atmos. Sci.*, **67**, 1655–1666, https://doi.org/10.1175/2009JAS3307.1.

Sakradzija, M., A. Seifert, and T. Heus, 2015: Fluctuations in a quasi-stationary shallow cumulus cloud ensemble. *Nonlinear Processes Geophys.*, **22**, 65–85, https://doi.org/10.5194/npg-22-65-2015.

——, ——, and A. Dipankar, 2016: A stochastic scale-aware parameterization of shallow cumulus convection across the convective gray zone. *J. Adv. Model. Earth Syst.*, **8**, 786–812, https://doi.org/10.1002/2016MS000634.

Siebesma, A. P., and J. Teixeira, 2000: An advection–diffusion scheme for the convective boundary layer: Description and 1D results. Preprints, *14th Symp. on Boundary Layers and Turbulence*, Aspen, CO, Amer. Meteor. Soc., 133–136.

——, and Coauthors, 2003: A large eddy simulation intercomparison study of shallow cumulus convection. *J. Atmos. Sci.*, **60**, 1201–1219, https://doi.org/10.1175/1520-0469(2003)60<1201:ALESIS>2.0.CO;2.

——, P. M. M. Soares, and J. Teixeira, 2007: A combined eddy-diffusivity mass-flux approach for the convective boundary layer. *J. Atmos. Sci.*, **64**, 1230–1248, https://doi.org/10.1175/JAS3888.1.

Soares, P. M. M., P. M. A. Miranda, A. P. Siebesma, and J. Teixeira, 2004: An eddy-diffusivity/mass-flux parametrization for dry and shallow cumulus convection. *Quart. J. Roy. Meteor. Soc.*, **130**, 3365–3383, https://doi.org/10.1256/qj.03.223.

Stull, R., 1988: *An Introduction to Boundary Layer Meteorology*. Springer, 670 pp.

Sukoriansky, S., B. Galperin, and I. Staroselsky, 2005: A quasi-normal scale elimination model of turbulent flows with stable stratification. *Phys. Fluids*, **17**, 085107, https://doi.org/10.1063/1.2009010.

——, ——, and V. Perov, 2006: A quasi-normal scale elimination model of turbulence and its application to stably stratified flows. *Nonlinear Processes Geophys.*, **13**, 9–22, https://doi.org/10.5194/npg-13-9-2006.

Sušelj, K., J. Teixeira, and G. Matheou, 2012: Eddy diffusivity/mass flux and shallow cumulus boundary layer: An updraft PDF multiple mass flux scheme. *J. Atmos. Sci.*, **69**, 1513–1533, https://doi.org/10.1175/JAS-D-11-090.1.

——, ——, and D. Chung, 2013: A unified model for moist convective boundary layers based on a stochastic eddy-diffusivity/mass-flux parameterization. *J. Atmos. Sci.*, **70**, 1929–1953, https://doi.org/10.1175/JAS-D-12-0106.1.

——, T. Hogan, and J. Teixeira, 2014: Implementation of a stochastic eddy-diffusivity/mass-flux parameterization into the Navy Global Environmental Model. *Wea. Forecasting*, **29**, 1374–1390, https://doi.org/10.1175/WAF-D-14-00043.1.

Teixeira, J., and P. Siebesma, 2000: A mass-flux/K-diffusion approach to the parameterization of the convective boundary layer: Global model results. Preprints, *14th Symp. on Boundary Layers and Turbulence*, Aspen, CO, Amer. Meteor. Soc., 231–234.

——, and S. Cheinet, 2004: A simple mixing length formulation for the eddy-diffusivity parameterization of dry convection. *Bound.-Layer Meteor.*, **110**, 435–453, https://doi.org/10.1023/B:BOUN.0000007230.96303.0d.

——, and C. A. Reynolds, 2008: Stochastic nature of physical parameterizations in ensemble prediction: A stochastic convection approach. *Mon. Wea. Rev.*, **136**, 483–496, https://doi.org/10.1175/2007MWR1870.1.

van Stratum, B. J. H., J. Vilá-Guerau de Arellano, C. C. van Heerwaarden, and H. G. Ouwersloot, 2014: Subcloud-layer feedbacks driven by the mass flux of shallow cumulus convection over land. *J. Atmos. Sci.*, **71**, 881–895, https://doi.org/10.1175/JAS-D-13-0192.1.

Wang, S., and B. Stevens, 2000: Top-hat representation of turbulence statistics in cloud-topped boundary layers: A large eddy simulation study. *J. Atmos. Sci.*, **57**, 423–441, https://doi.org/10.1175/1520-0469(2000)057<0423:THROTS>2.0.CO;2.

Witek, M. L., J. Teixeira, and G. Matheou, 2011a: An eddy diffusivity–mass flux approach to the vertical transport of turbulent kinetic energy in convective boundary layers. *J. Atmos. Sci.*, **68**, 2385–2394, https://doi.org/10.1175/JAS-D-11-06.1.

——, ——, and ——, 2011b: An integrated TKE-based eddy-diffusivity/mass-flux boundary layer closure for the dry convective boundary layer. *J. Atmos. Sci.*, **68**, 1526–1540, https://doi.org/10.1175/2011JAS3548.1.

Brought to you by NOAA Central Library | Unauthenticated | Downloaded 03/07/22 07:40 PM UTC